RASSF4 controls SOCE and ER–PM junctions through regulation of PI(4,5)P_2

Yu-Ju Chen, Chi-Lun Chang, Wan-Ru Lee, and Jen Liou

Department of Physiology, University of Texas Southwestern Medical Center, Dallas, TX

RAS association domain family 4 (RASSF4) is involved in tumorigenesis and regulation of the Hippo pathway. In this study, we identify new functional roles of RASSF4. First, we discovered that RASSF4 regulates store-operated Ca^{2+} entry (SOCE), a fundamental Ca^{2+} signaling mechanism, by affecting the translocation of the endoplasmic reticulum (ER) Ca^{2+} sensor stromal interaction molecule 1 (STIM1) to ER–plasma membrane (PM) junctions. It was further revealed that RAS SF4 regulates the formation of ER–PM junctions and the ER–PM tethering function of extended synaptotagmins E-Syt2 and E-Syt3. Moreover, steady-state PM phosphatidylinositol 4,5-bisphosphate (PI[4,5]P_2) levels, important for localization of STIM1 and E-Syts at ER–PM junctions, were reduced in *RASSF4*-knockdown cells. Furthermore, we demonstrated that RASSF4 interacts with and regulates the activity of adenosine diphosphate ribosylation factor 6 (ARF6), a small G protein and upstream regulator of type I phosphatidylinositol phosphate kinases (PIP5Ks) and PM PI(4,5)P_2 levels. Overall, our study suggests that RASSF4 controls SOCE and ER–PM junctions through ARF6-dependent regulation of PM PI(4,5)P_2 levels, pivotal for a variety of physiological processes.

Introduction

Phosphatidylinositol 4,5-bisphosphate (PI[4,5]P_2) is an inositol-containing phospholipid enriched at the inner leaflet of the plasma membrane (PM; Balla, 2013). PI(4,5)P_2 governs many cellular processes including membrane traffic, ion transport activities, and cytoskeleton–PM interactions. Aberrant metabolism of PI(4,5)P_2 has been associated with cancer, oculocerebrorenal syndrome of Lowe, and infectious diseases (Bunney and Katan, 2010; Balla, 2013; Staiano et al., 2015). Most PI(4,5)P_2 is generated by type I phosphatidylinositol phosphate kinases (PIP5Ks), which phosphorylate the 5-position of the inositol ring of phosphatidylinositol 4-phosphate (PI[4]P; Roth, 2004). The activity and localization of PIP5Ks are regulated by multiple factors including ADP ribosylation factor 6 (ARF6), a small G protein that dynamically cycles between the inactive GDP-bound (ARF6-GDP) and the active GTP-bound (ARF6-GTP) states (van den Bout and Divecha, 2009). ARF6-GTP directly activates PIP5Ks to control the generation of PI(4,5)P_2 (Honda et al., 1999; Brown et al., 2001).

In addition to its many functions in resting cells, PM PI(4,5)P_2 is essential for Ca^{2+} signaling in receptor-stimulated cells (Chang and Liou, 2016). Receptor-activated PLC hydrolyzes PM PI(4,5)P_2 to generate soluble inositol triphosphate (IP_3), triggering Ca^{2+} release from the ER. Depletion of ER Ca^{2+} activates Ca^{2+} influx across the PM, a process known as store-operated Ca^{2+} entry (SOCE), essential for a wide array of cellular functions (Prakriya and Lewis, 2015). Defective SOCE is associated with many human diseases, including severe combined immunodeficiency, cardiac hypertrophy, and cancer (Bergmeier et al., 2013).

The mediators of SOCE, stromal interaction molecule 1 (STIM1) and Orai1, were identified using RNA interference screens (Liou et al., 2005; Roos et al., 2005; Feske et al., 2006; Vig et al., 2006; Zhang et al., 2006). STIM1 is a single-pass ER membrane protein that binds Ca^{2+} at steady state. ER Ca^{2+} depletion triggers conformational change of STIM1 to expose the Orai1-activating domain and the PM-targeting polybasic motif in its C-terminal cytosolic region (Liou et al., 2007; Walsh et al., 2010; Zhou et al., 2013; Maus et al., 2015). The exposed polybasic tail of STIM1 binds PI(4,5)P_2 at the PM. As a result, STIM1 accumulates at ER–PM junctions, where the ER closely opposes the PM within a 30-nm gap distance (Wu et al., 2006; Liou et al., 2007; Walsh et al., 2010; Henne et al., 2015). Localization at ER–PM junctions enables STIM1 interaction with the PM Ca^{2+} channel Orai1 and activation of SOCE (Luik et al., 2006).

Besides SOCE, PM PI(4,5)P_2 is important for ER–PM junction formation. The best-characterized proteins mediating

Correspondence to Jen Liou: jen.liou@utsouthwestern.edu

Abbreviations used: ARF6, ADP ribosylation factor 6; ECB, extracellular buffer; EM, electron microscopy; FKBP, FK506-binding protein; FRB, FKBP-rapamycin binding; HUVEC, human umbilical vein endothelial cell; MAPPER, membrane-attached peripheral ER; NFAT, nuclear factor of activated T cells; NGS, normal goat serum; ORP, oxysterol-binding protein–related protein; PI(4)P, phosphatidylinositol 4-phosphate; PI(4,5)P_2, phosphatidylinositol 4,5-bisphosphate; PIP5K, type I phosphatidylinositol phosphate kinases; PM, plasma membrane; RAS SF4, RAS association domain family 4; SARAH, Salvador-RASSF-Hippo; SOCE, store-operated Ca^{2+} entry; TG, thapsigargin; TIRF, total internal reflection fluorescence; TIRFM, TIRF microscopy; STIM1, stromal interaction molecule 1.

The Rockefeller University Press
J. Cell Biol. Vol. 216 No. 7 2011–2025
https://doi.org/10.1083/jcb.201606047

the formation of ER–PM junctions in mammalian cells are extended synaptotagmins E-Syt2 and E-Syt3 (Giordano et al., 2013). E-Syt2 and E-Syt3 are ER membrane proteins containing multiple C2 domains. Interaction of the very C-terminal C2 domain of E-Syt2 and E-Syt3 with PM $PI(4,5)P_2$ mediates ER tethering to the PM at ER–PM junctions.

Here, we identified RAS association domain family 4 (RASSF4) from a human siRNA screen for regulators of SOCE. Subsequently, we showed that RASSF4 functions as a novel regulator of PM $PI(4,5)P_2$, affecting not only SOCE, but also ER–PM junctions. RASSF4 belongs to the RASSF family of proteins containing a RAS association (RA) domain and a Salvador-RASSF-Hippo (SARAH) domain in the C terminus (Chan et al., 2013). The RA domain of RASSF4 is predicted to interact with small G proteins (Sherwood et al., 2010). The SARAH domain can mediate dimerization and protein–protein interactions (Scheel and Hofmann, 2003; Dittfeld et al., 2012; Makbul et al., 2013). RASSF4 associates with MST1, the mammalian orthologue of the *Drosophila* Hippo protein, and inhibits the Hippo pathway (Crose et al., 2014). Altered expression of *RASSF4* is frequently associated with the progression of many cancer types, including nasopharyngeal, lung, head, and neck cancers, as well as alveolar rhabdomyosarcoma (Chow et al., 2004; Steinmann et al., 2009; Crose et al., 2014; Han et al., 2016). By dissecting the mechanism underlying RASSF4-mediated control of PM $PI(4,5)P_2$ levels, we found that RASSF4 interacts with and regulates the activation of ARF6, an upstream regulator of PIP5Ks and PM $PI(4,5)P_2$. Overall, our study reveals novel functional roles of RASSF4 and provides new insights into the regulation of $PI(4,5)P_2$, Ca^{2+} signaling, and ER–PM junctions.

Results

Identification of RASSF4 as a positive regulator of SOCE

The key regulators of SOCE, STIM1 and STIM2, were identified from a screen for siRNAs inhibiting sustained Ca^{2+} signaling in HeLa cells stimulated with histamine and thapsigargin (TG) to deplete ER Ca^{2+} and activate SOCE (Liou et al., 2005). Another hit from this screen was RASSF4 (Fig. 1 A). Similar to siRNA targeting *STIM1* (siSTIM1), siRASSF4 suppressed the sustained phase but not the initial peak of the Ca^{2+} response in stimulated HeLa cells (Fig. 1 B). To further characterize and validate the effect of RASSF4 on Ca^{2+} responses, two additional diced siRNA pools targeting the coding sequence of the N-terminal region (siRASSF4_N') and the C-terminal region (siRASSF4_C') of human RASSF4 protein (Fig. 1 A) were generated. We implemented a Ca^{2+} add-back experiment that enables separate monitoring of Ca^{2+} release from intracellular stores and the subsequent Ca^{2+} flux across the PM in HeLa cells treated with either siRASSF4_N' or siRASSF4_C'. Reduced Ca^{2+} flux across the PM was observed in cells treated with either siRASSF4_N' or siRASSF4_C', with no apparent effect on release of stored Ca^{2+} (Fig. 1 C). Moreover, expression of a RAS SF4 construct fused with YFP rescued the suppressed Ca^{2+} flux across the PM in cells treated with a diced siRNA pool targeting the 3′ untranslated region of *RASSF4* (Fig. S1 A). These data, derived using four different siRNAs targeting *RASSF4*, support the specificity of *RASSF4* knockdown and a selective regulation of Ca^{2+} flux after store depletion by RASSF4.

We further tested the effect of *RASSF4* knockdown on SOCE in primary human umbilical vein endothelial cells (HUVECs) and noncancerous retinal pigment epithelial 1 (RPE1) cells. Results similar to those in HeLa cells were obtained (Fig. 1, D and E; and Fig. S1, B and C), indicating that the effect of RASSF4 on SOCE is not confined to HeLa cells. The effect of RASSF4 on SOCE was supported by measuring the quenching of intracellular Fura-2 fluorescence by influx of Mn^{2+}, a surrogate for Ca^{2+}. Consistent with a role of RASSF4 in regulating Ca^{2+} influx, siRASSF4-treated cells exhibited suppressed Mn^{2+} quench rate triggered by TG (Fig. 1 F). Furthermore, we tested the effect of *RASSF4* knockdown on the activation of nuclear factor of activated T cells (NFAT), a transcription factor activated by SOCE and essential for many physiological processes (Hogan et al., 2003), in TG-treated cells. The percentage of cells with nuclear translocation of NFAT, indicative of NFAT activation, was significantly reduced in siRASSF4-treated cells (Fig. 1 G). Together, these results demonstrate the importance of RASSF4 in the activation of SOCE and its downstream signaling events.

SOCE is activated by interaction of STIM1 and Orai1 at ER–PM junctions. Therefore, the effect of *RASSF4* knockdown on SOCE could be caused by dysregulation of STIM1, Orai1, and/or ER–PM junctions. However, we found that the expression levels of STIM1 and Orai1 proteins were not affected in siRASSF4-treated cells (Fig. S1 D). In addition, knockdown of *RASSF4* did not affect the expression of several other genes implicated in regulating SOCE (Fig. S1 E). Thus, we examined the function of Orai1 in siRASSF4-treated cells using a soluble fragment of the STIM1 C-terminus (STIM1-CT) that can activate Orai1 and mediate constitutive Ca^{2+} influx without localizing to ER–PM junctions (Sharma et al., 2013). Knockdown of *RASSF4* did not affect Orai1 activation by STIM1-CT (Fig. 1 H). In contrast, knockdown of *RASSF4* resulted in a reduction of SOCE in STIM1-overexpressing cells (Fig. 1 I), indicating that RASSF4 regulates STIM1 activation during SOCE. Therefore, the reduced SOCE observed in siRASSF4-treated cells is likely caused by impaired STIM1 activation and/or defects in ER–PM junctions.

RASSF4 regulates STIM1 localization at ER–PM junctions

To determine the effect of RASSF4 on STIM1 activation, confocal microscopy was applied to monitor the dynamic localization of STIM1 after ER Ca^{2+} depletion. TG-induced STIM1 accumulation at ER–PM junctions, which appears as puncta formation, was significantly suppressed in siRASSF4-treated cells (Fig. 2 A and Video 1). These observations were confirmed using total internal reflection fluorescence (TIRF) microscopy (TIRFM; Fig. 2 B), which allows for selective illumination of fluorescent probes within ∼100 nm of the PM (Steyer and Almers, 2001). These results indicate a defect in STIM1 translocation to ER–PM junctions in *RASSF4*-knockdown cells. Conversely, RASSF4 overexpression enhanced STIM1 accumulation at ER–PM junctions induced by TG (Fig. 2 C). Together, these results demonstrate that RASSF4 regulates the activation of STIM1 during SOCE.

To further dissect the mechanism underlying RASSF4 regulation of STIM1 activation, we used a constitutively active STIM1-D76A construct that contains a point mutation disrupting the key Ca^{2+}-binding residue in its luminal EF hand, adopts the activated conformation, and readily localizes at ER–PM junctions at steady state (Liou et al., 2005). The activated

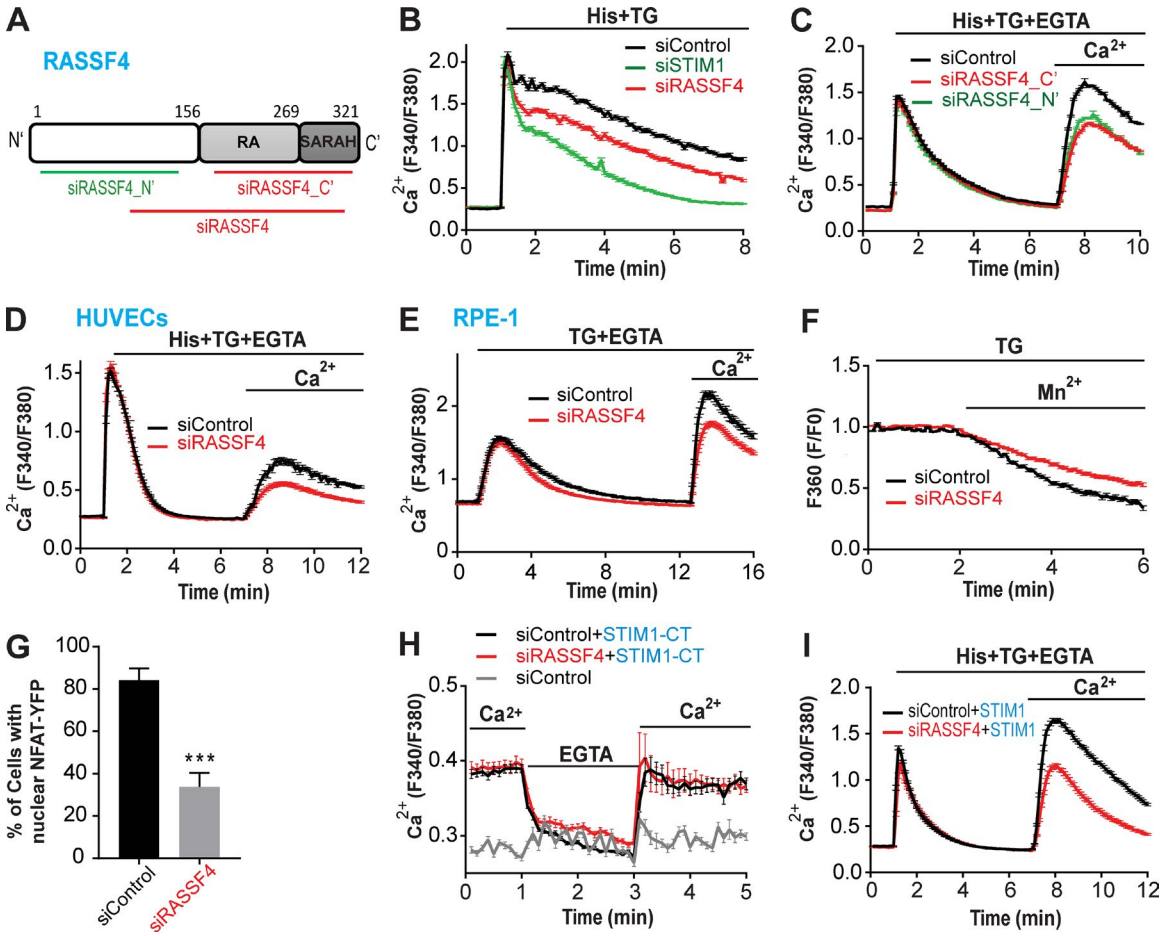

Figure 1. **RASSF4 is a positive regulator of SOCE.** (A) A diagram of the domain structure of RASSF4. The regions targeted by siRASSF4_N' used in C, siRASSF4_C' used in C, and siRASSF4 used in B are indicated. RA, RAS association. (B) Intracellular Ca^{2+} levels determined by analysis of Fura-2 fluorescence ratios in HeLa cells treated with a control siRNA (siControl), siSTIM1, or siRASSF4 and stimulated with 1 µM TG and 100 µM histamine (His). Shown are mean Fura-2 ratios ± SEM of >300 cells for each condition. Similar results were obtained from >10 independent experiments. (C) Fura-2 ratios of HeLa cells treated with the indicated siRNAs. Cells were stimulated with 1 µM TG, 100 µM His, and 2 mM EGTA; 2 mM Ca^{2+} was added 6 min after stimulation. Shown are mean Fura-2 ratios ± SEM derived from >1,000 cells for each condition across two independent experiments. (D) Fura-2 ratios of siRNA-treated HUVECs stimulated as described in C. Shown are mean Fura-2 ratios ± SEM derived from >500 cells for each condition across two independent experiments. (E) Fura-2 ratios of RPE-1 cells treated with the indicated siRNAs. Cells were stimulated with 1 µM TG and 2 mM EGTA; 2 mM Ca^{2+} was added 11.5 min after stimulation. Shown are mean Fura-2 ratios ± SEM of >280 cells for each condition. Similar results were obtained from three independent experiments. (F) Mn^{2+} influx measured by Fura-2 quenching in siRNA-treated HeLa cells stimulated with 1 µM TG. Shown are means ± SEM derived from >200 cells for each condition across two independent experiments. (G) HeLa cells were sequentially transfected with NFAT-YFP, and either siControl or siRASSF4 was treated with 1 µM TG for 10 min and scored for NFAT by fluorescence imaging. Percentage of cells with nuclear translocation of NFAT was calculated from 80–100 cells across three independent experiments. Means ± SEM are plotted. ***, $P < 0.001$. (H) HeLa cells were treated with siControl and a control vector, siControl and mCherry-STIM1-CT, or siRASSF4 and mCherry-STIM1-CT. Ca^{2+} was chelated using 2 mM EGTA, and then 2 mM Ca^{2+} was added to evaluate spontaneous Ca^{2+} influx. Mean Fura-2 ratios ± SEM of >500 cells across three independent experiments are plotted. (I) Fura-2 ratios in mCherry-STIM1–expressing HeLa cells treated with either siRASSF4 or siControl. Cells were stimulated as described in C. Shown are mean traces of >300 cells for each condition from a representative of three independent experiments.

Ca^{2+} influx caused by expressing STIM1-D76A was reduced in siRASSF4-treated cells (Fig. 3 A). Conversely, overexpression of RASSF4 enhanced Ca^{2+} influx induced by the expression of STIM1-D76A (Fig. 3 B). Consistent with these Ca^{2+} data, steady-state localization of STIM1-D76A at ER–PM junctions, measured by the density of STIM1-D76A puncta detected using TIRFM, was significantly decreased in siRASSF4-treated cells (Fig. 3 C). These results indicate that, even in the activated conformation, STIM1 fails to accumulate at ER–PM junctions to mediate Ca^{2+} influx. Moreover, overexpression of RASSF4 increased the density of steady-state STIM1-D76A puncta (Fig. 3 D), demonstrating that RASSF4 has a dominant effect over STIM1 and suggesting that RASSF4 regulates STIM1 localization at ER–PM junctions rather than its conformational change. Furthermore, time-lapse TIRFM imaging of stationary HeLa cells revealed that STIM1-D76A puncta were less stable in siRASSF4-treated cells than in control cells (Fig. 3 E). These results raise the possibility that both STIM1 activation and ER–PM junctions are defective in *RASSF4*-knockdown cells.

RASSF4 regulates the formation and stability of ER–PM junctions

Previous studies indicate that ER–PM junctions exist before the activation of SOCE (Wu et al., 2006), and STIM1 reversibly localizes to these loci depending on ER Ca^{2+} levels (Liou et al., 2005). We used electron microscopy (EM) to examine the effect of RASSF4 on the formation of ER–PM junctions in cells at steady state. ER–PM junctions were identified as tubules with

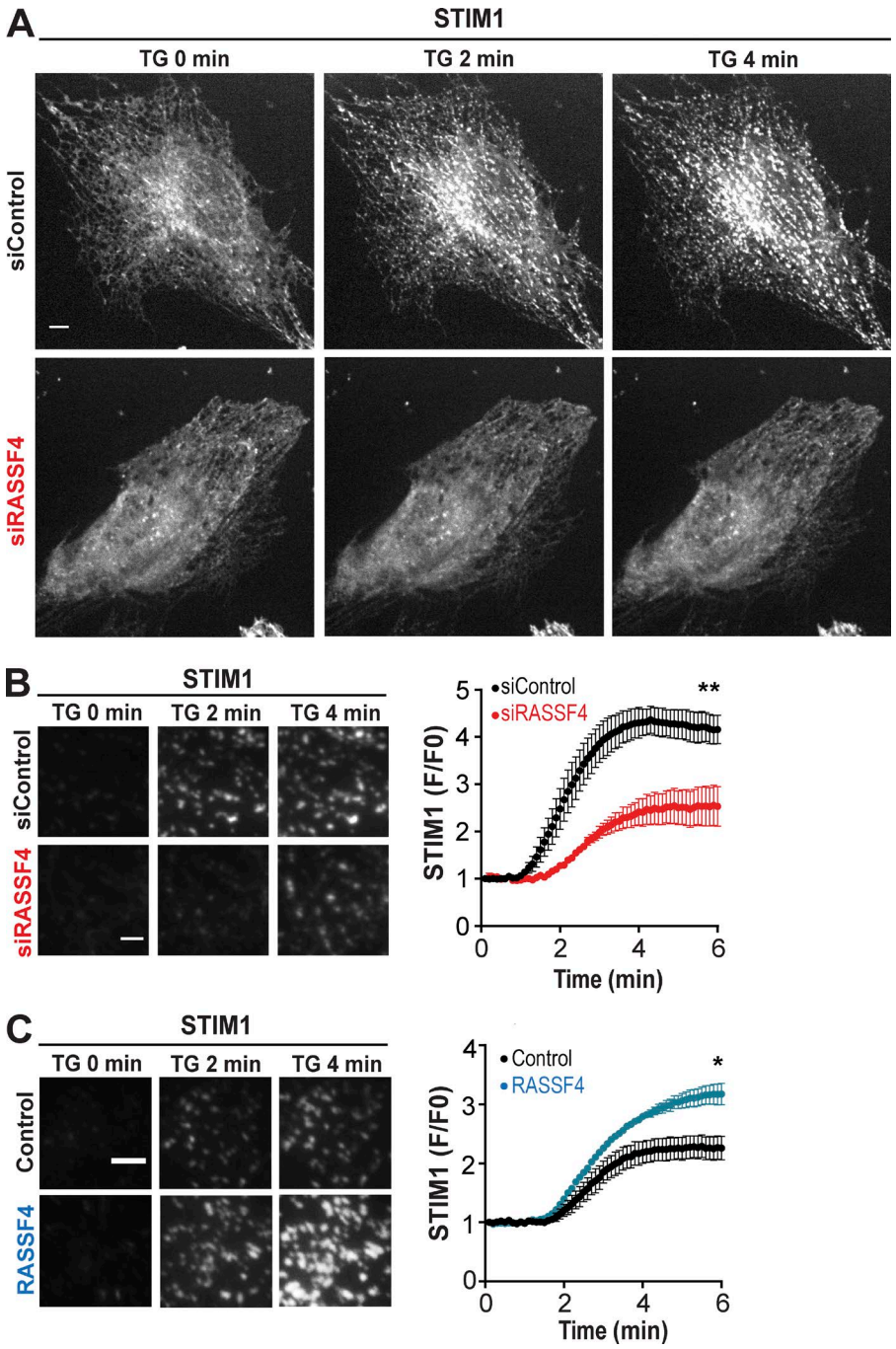

Figure 2. **RASSF4 regulates STIM1 translocation to ER–PM junctions after ER Ca^{2+} depletion.** (A) HeLa cells cotransfected with mCherry-STIM1 and either siControl or siRASSF4 were imaged by confocal microscopy. 1 µM TG was used for stimulation. Bar, 5 µm. (B) mCherry-STIM1 translocation to ER–PM junctions monitored by TIRFM in 1-µM TG–stimulated HeLa cells cotransfected with mCherry-STIM1 and either siControl or siRASSF4. Bar, 2 µm. The plot of mCherry-STIM1 intensity is from >12 cells for each condition across three independent experiments analyzed. Means ± SEM are plotted. **, $P < 0.01$. (C) HeLa cells cotransfected with mCherry-STIM1 and either RASSF4-YFP or a control vector were treated with 1 µM TG and monitored by TIRFM. Bar, 2 µm. The plot of mCherry-STIM1 intensity over time is from >12 cells for each condition across three independent experiments. Means ± SEM are plotted. *, $P < 0.05$.

ER-targeted HRP (HRP-ER) located within 50 nm of the PM (Wu et al., 2006). The percentage of PM length engaged in contact with the ER was calculated. Approximately 3.3% of the PM was occupied by the ER in control cells, compared with ∼1.6% in *RASSF4*-knockdown cells (Fig. 4 A). In contrast, overexpression of RASSF4 increased the PM occupancy of the ER to ∼4.8% (Fig. 4 B). These EM results reveal that RASSF4 regulates the formation of ER–PM junctions in cells at steady state. We validated the EM results using ER labeling in live cells imaged by time-lapse TIRFM to measure ER–PM junctions (Chang et al., 2013). The density of ER–PM junctions in siRASSF4-treated cells was reduced to ∼50% of that in control cells (Fig. 4 C). Conversely, overexpression of RASSF4 significantly increased the density of ER–PM junctions (Fig. 4 D). Together, these results show that RASSF4 regulates the formation of ER–PM junctions in cells at steady state.

Our group has previously developed a genetically encoded marker named MAPPER (membrane-attached peripheral ER) that selectively labels ER–PM junctions (Chang et al., 2013). Using MAPPER, similar reduction in the density of ER–PM junctions was observed in *RASSF4*-knockdown cells (Fig. S2). Unlike the EM or the ER-labeling approach, MAPPER enables tracking of individual ER–PM junctions in real time and, thus, can be used to further determine the stability of single ER–PM junctions. By monitoring MAPPER-labeled ER–PM junctions in stationary HeLa cells, we observed that the percentage of stable ER–PM junctions was reduced in siRASSF4-treated cells (Fig. 4 E). Overall, the

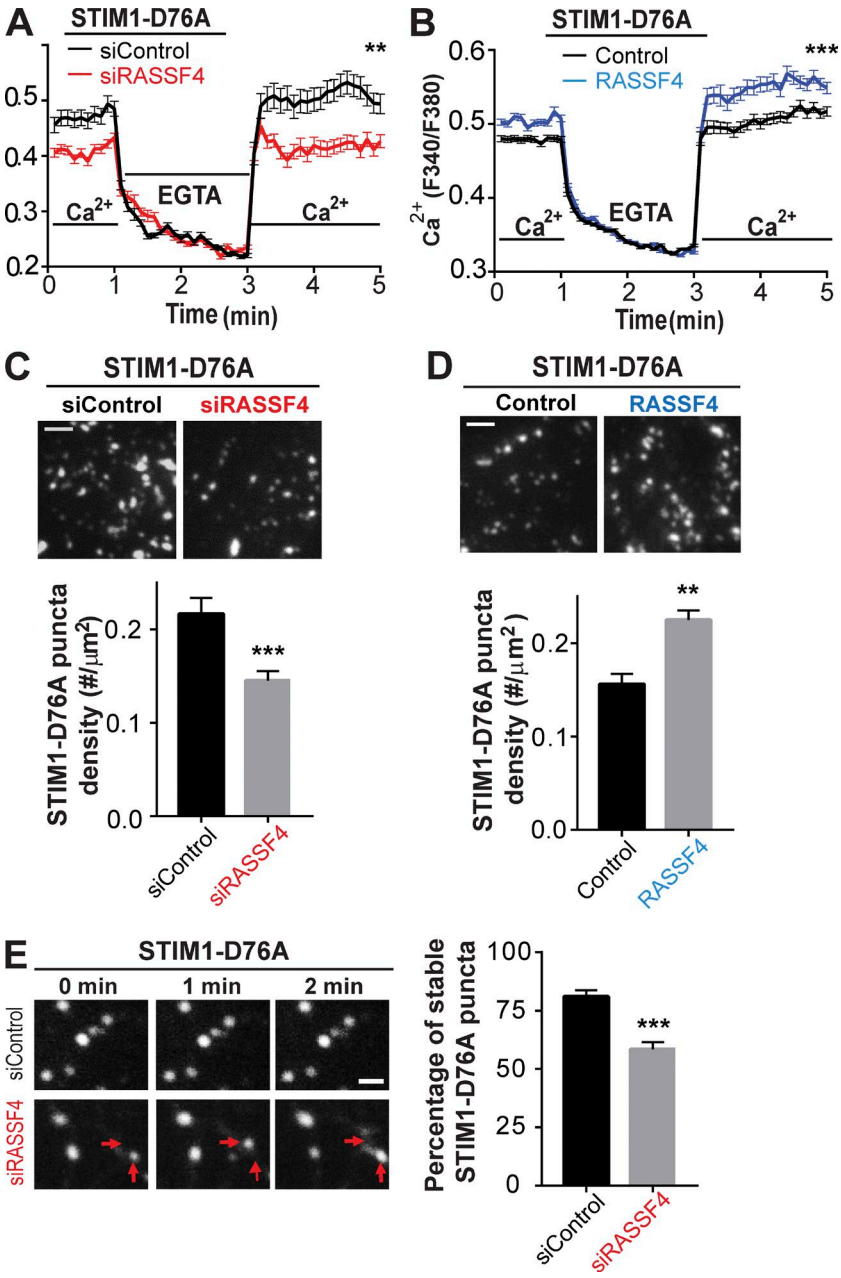

Figure 3. **RASSF4 regulates STIM1-D76A–mediated Ca^{2+} influx and its localization at ER–PM junctions.** (A) HeLa cells were treated with siRASSF4 or siControl for 2 d and then were transfected with mCherry-STIM1-D76A. After 12 h, Ca^{2+} was chelated by 2 mM EGTA followed by addition of 2 mM Ca^{2+}. Fura-2 ratios were determined as a function of time. Means ± SEM of >300 cells are plotted. (B) HeLa cells were transfected with mCherry-STIM1-D76A and RASSF4-YFP or a control vector. After 12 h, Ca^{2+} was chelated by 2 mM EGTA followed by addition of 2 mM Ca^{2+}. Fura-2 ratios were determined as a function of time. Means ± SEM of >800 cells are plotted. (C) HeLa cells cotransfected with mCherry-STIM1-D76A and either siControl or siRASSF4 were monitored by TIRFM. Bar, 2 µm. The density of mCherry-STIM1-D76A puncta was quantified. (D) TIRF images of HeLa cells cotransfected with mCherry-STIM1-D76A and either a control vector or RASSF4-YFP. Bar, 2 µm. The density of mCherry-STIM1-D76A puncta was quantified. (C and D) Means ± SEM of 20 cells for each condition across two independent experiments are shown. (E) TIRF images of HeLa cells treated with siRASSF4 or siControl and then transfected with mCherry-STIM1-D76A. Red arrows indicate unstable STIM1-D76A puncta. Bar, 1 µm. The percentage of stable STIM1-D76A puncta was quantified. Approximately 500 puncta from six different cells for each condition across three independent experiments were analyzed. Means ± SEM are plotted. **, $P < 0.01$; ***, $P < 0.001$.

results derived using three independent yet complimentary assays for ER–PM junctions demonstrate that RASSF4 regulates the formation as well as the stability of ER–PM junctions in cells at steady state.

The ER membrane proteins E-Syt2 and E-Syt3 contribute to the formation of steady-state ER–PM junctions by binding to PM $PI(4,5)P_2$ (Giordano et al., 2013). We tested the dependence of RASSF4 on the ER–PM tethering function of E-Syt2 and E-Syt3 by examining GFP–E-Syt2 and GFP–E-Syt3 puncta using TIRFM. Knockdown of *RASSF4* reduced the density of GFP–E-Syt2 and GFP–E-Syt3 puncta (Fig. 5, A and B), indicating a dominant effect of RASSF4 over E-Syt2 and E-Syt3 on the formation of ER–PM junctions. Furthermore, overexpression of RASSF4 had an additive effect on the formation of ER–PM junctions in cells overexpressing E-Syt2 or E-Syt3 (Fig. 5, C and D). Therefore, RASSF4 not only regulates SOCE mediated by STIM1 at ER–PM junctions in ER Ca^{2+}-depleted cells, but also regulates the formation of ER–PM junctions mediated by E-Syt2 and E-Syt3 in cells at steady state.

RASSF4 regulates PM $PI(4,5)P_2$ levels in cells at steady state and after receptor stimulation

Given the critical role of PM $PI(4,5)P_2$ in governing the localization of STIM1, E-Syt2, and E-Syt3 at ER–PM junctions, we tested the effect of RASSF4 on PM $PI(4,5)P_2$. First, we used a biosensor, PLCδ-PH (Stauffer et al., 1998), to detect steady-state $PI(4,5)P_2$ levels at the PM using confocal microscopy. A significant reduction in the relative intensity of PLCδ-PH at the PM, indicative of reduced PM $PI(4,5)P_2$ levels, was observed in siRASSF4-treated cells (Fig. 6 A). Using another $PI(4,5)P_2$ biosensor, Tubby-GFP (Quinn et al., 2008), similar results were obtained (Fig. S3 A). In addition, siRASSF4-treated cells exhibited a decrease in total $PI(4,5)P_2$ levels directly measured

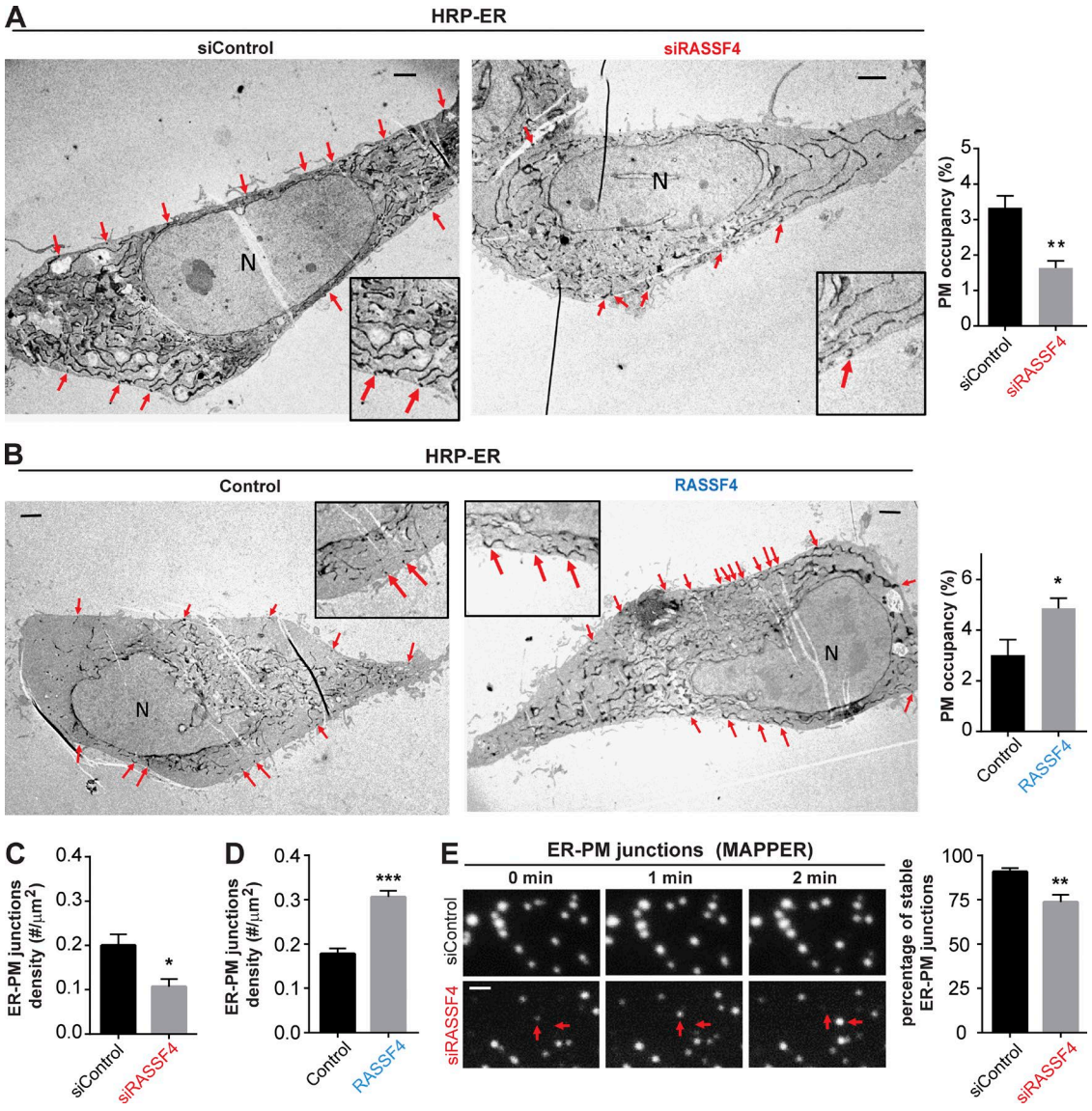

Figure 4. **RASSF4 regulates the formation and stability of ER–PM junctions.** (A and B, left) EM micrographs of HRP-KDEL–expressing HeLa cells treated with the indicated siRNA or plasmid for 2 d. Red arrows indicate ER–PM junctions. Bar, 2 µm. (Right) The percentage of PM length engaged in contact with the ER is shown. Means ± SEM of six to eight cells are plotted. N indicates the cell nucleus. (C and D) Densities of ER–PM junctions determined using a TIRF image series of YFP-KDEL–expressing HeLa cells that were treated with siRASSF4 or siControl (C) or transfected with RASSF4 or a control vector (D). More than 24 cells for each condition across three independent experiments were analyzed. Means ± SEM are plotted. (E) TIRF images of ER–PM junctions labeled by MAPPER in cells treated with siControl or siRASSF4. Red arrows indicate unstable junctions. Bar, 1 µm. The percentage of stable ER–PM junctions labeled by MAPPER was quantified. More than 500 puncta in six different cells for each condition were evaluated. Means ± SEM are shown. *, $P < 0.05$; **, $P < 0.01$; ***, $P < 0.001$.

using *myo*-[^{3}H]inositol to label phosphoinositides (Fig. 6 B). Moreover, direct staining of PI(4,5)P_2 at the PM with an antibody, using a protocol established previously (Hammond et al., 2009), confirmed the reduction of PM PI(4,5)P_2 in *RASSF4*-knockdown cells (Fig. 6 C). In contrast, overexpression of RAS SF4 resulted in an increase in steady-state PI(4,5)P_2 levels at the PM (Fig. 6 D). These results demonstrate that RASSF4 regulates PM PI(4,5)P_2 levels in resting cells.

In receptor-stimulated cells, PM PI(4,5)P_2 is hydrolyzed by PLC to generate IP_3 and diacylglycerol for activation of downstream signaling events. The levels of PM PI(4,5)P_2 are rapidly restored via a feedback pathway coupling PI(4,5)P_2 hydrolysis to its replenishment (Chang and Liou, 2016). The replenishment of PM PI(4,5)P_2 after receptor-stimulated hydrolysis was suppressed in *RASSF4*-knockdown cells (Fig. 6 E). Conversely, RASSF4 overexpression augmented the replenishment of PM PI(4,5)P_2 (Fig. 6 F). These results demonstrate that RASSF4 is not only important for maintaining PM PI(4,5)P_2 levels in cells at steady state, but also essential for replenishing PM PI(4,5)P_2 after its hydrolysis in receptor-stimulated cells.

RASSF4 regulates the levels of PI(4)P and PIP5Ks at the PM

Reduction in PM PI(4,5)P_2 in siRASSF4-treated cells might arise from insufficient precursors. The levels of PI(4)P, an immediate precursor of PI(4,5)P_2, at the PM were examined using a biosensor, N-PH-ORP5 (Chung et al., 2015), in cells at steady state. In contrast to the reduced PM PI(4,5)P_2 levels, an increase

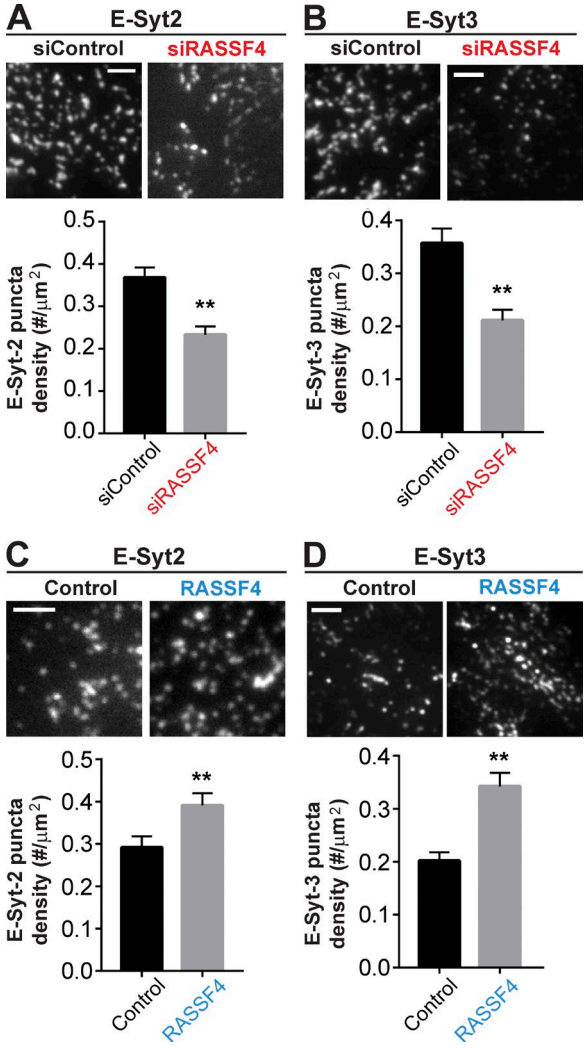

Figure 5. **RASSF4 regulates the localization of E-Syt2 and E-Syt3 at ER–PM junctions.** (A) Localization of GFP–E-Syt2 monitored by TIRFM in siControl- or siRASSF4-treated HeLa cells. The density of GFP–E-Syt2 puncta in 20 cells across two independent experiments was quantified. Means ± SEM are plotted. (B) Localization of GFP–E-Syt3 monitored by TIR FM in siControl- or siRASSF4-treated HeLa cells. GFP–E-Syt3 puncta density in 20 cells from two independent experiments was quantified. Means ± SEM are plotted. (C) GFP–E-Syt2 at ER–PM junctions monitored by TIRFM in HeLa cells cotransfected with a control vector or RASSF4. The density of GFP–E-Syt2 puncta in 20 cells across two independent experiments was quantified. Means ± SEM are shown. (D) GFP–E-Syt3 at ER–PM junctions monitored by TIRFM in HeLa cells transfected with an empty vector or a vector for expression of RASSF4. GFP–E-Syt3 puncta density in 20 cells from two independent experiments was quantified. Means ± SEM are shown. **, $P < 0.01$. Bars, 2 μm.

in PM PI(4)P was detected in siRASSF4-treated cells compared with control cells (Fig. 7 A). Similar results were obtained using PH-Osh2×2 (Roy and Levine, 2004; Balla et al., 2008), another biosensor for PI(4)P (Fig. S3 B). Increase in PM PI(4)P levels in siRASSF4-treated cells was further confirmed by immunostaining using an anti-PI(4)P antibody (Fig. 7 B). The increased PI(4)P at the PM suggests that $PI(4,5)P_2$ generation from PI(4)P by PIP5Ks is suppressed in *RASSF4*-knockdown cells.

PIP5K1B and PIP5K1C are two isoforms of PIP5Ks localized at the PM and linked to the regulation of $PI(4,5)P_2$ levels and Ca^{2+} signaling in HeLa cells (Padrón et al., 2003; Wang et al., 2004). Using confocal microscopy, it was revealed that PM localization of both PIP5K1B and PIP5K1C was suppressed in siRASSF4-treated cells (Fig. 7 C and Fig. S3 C). These results suggest that altered localization of PIP5Ks might be the cause of defective PM $PI(4,5)P_2$ levels, ER–PM junctions, and SOCE in *RASSF4*-knockdown cells. To test this hypothesis, we applied a previously established rapamycin-inducible approach (Suh et al., 2006) in which a FK506-binding protein (FKBP)–fused PIP5K1C (FKBP-PIP5K) is acutely recruited to the PM-localized FKBP-rapamycin binding (FRB) protein (Lyn-FRB) via heterodimerization to increase PM $PI(4,5)P_2$ levels (Fig. 7 D). A kinase-dead mutant, FKBP-PIP5Ki, was used as a negative control. Addition of rapamycin induced a rapid translocation of FKBP-PIP5K or the control FKBP-PIP5Ki to the PM in cells cotransfected with Lyn-FRB (Fig. S4 A). Consistent with previous findings (Suh et al., 2006), acute recruitment of PIP5K to the PM increased PM $PI(4,5)P_2$ levels in siControl-treated cells (Fig. 7 E, black bar vs. red bar). Notably, the acute recruitment of PIP5K to the PM was sufficient to overcome the deficiency of RASSF4 and restored PM $PI(4,5)P_2$ levels in siRASSF4-treated cells (Fig. 7 E, gray bar vs. green bar). In addition, reduction in ER–PM junctions, measured using either ER labeling or MAPPER, was restored in siRASSF4-treated cells by induced targeting of PIP5K to the PM (Fig. 7 F and Fig. S4 B). Moreover, the impaired TG-triggered STIM1 translocation to ER–PM junctions, as determined by STIM1 puncta density, and SOCE were restored in siRASSF4-treated cells after induced PM targeting of PIP5K (Fig. S4 C and Fig. 7 G). Thus, the various defects in *RASSF4*-knockdown cells can be rescued by targeting PIP5K to the PM to increase PM $PI(4,5)P_2$. Together, these results suggest that RASSF4 regulates PIP5Ks to control $PI(4,5)P_2$ levels at the PM.

RASSF4 interacts with ARF6 and regulates its localization and activation

The small G protein ARF6 can directly activate PIP5Ks and regulate PM localization of PIP5Ks as well as $PI(4,5)P_2$ production (Honda et al., 1999). ARF6 is partially localized at the PM (Donaldson and Honda, 2005). In siRASSF4-treated cells, a dramatic accumulation of ARF6 in large internal structures with reduced localization at the PM was observed (Fig. 8 A). This altered distribution of ARF6 is reminiscent of the internal structures formed by prolonged expression of ARF6-T27N, an ARF6 mutant that remains in the inactive GDP-bound state (Peters et al., 1995). This observation suggests a defect of ARF6 activation in siRASSF4-treated cells. Consistent with this notion, a reduction of ARF6 in the active ARF6-GTP state was observed in siRASSF4-treated cells compared with control cells (Fig. 8 B), indicating that RASSF4 regulates the localization and activation of ARF6.

To address the mechanism by which RASSF4 regulates ARF6 activation, we examined the subcellular localization of RASSF4-YFP using confocal microscopy and found that RASSF4 is diffusely distributed in the cytoplasm of HeLa cells (Fig. S5). As RASSF4 was predicted to bind small G proteins (Sherwood et al., 2010), it is plausible that RASSF4 binds ARF6 and regulates its activation. Indeed, RASSF4 was detected in the immunoprecipitation of ARF6 (Fig. 8 C). Reciprocally, ARF6 was detected in the immunoprecipitation of RASSF4 (Fig. 8 D), indicating that RASSF4 interacts with ARF6.

ARF6 dynamically switches between GTP-bound and GDP-bound states to perform its functions (Honda et al., 1999; Wong and Isberg, 2003). Several ARF6 mutants mimicking

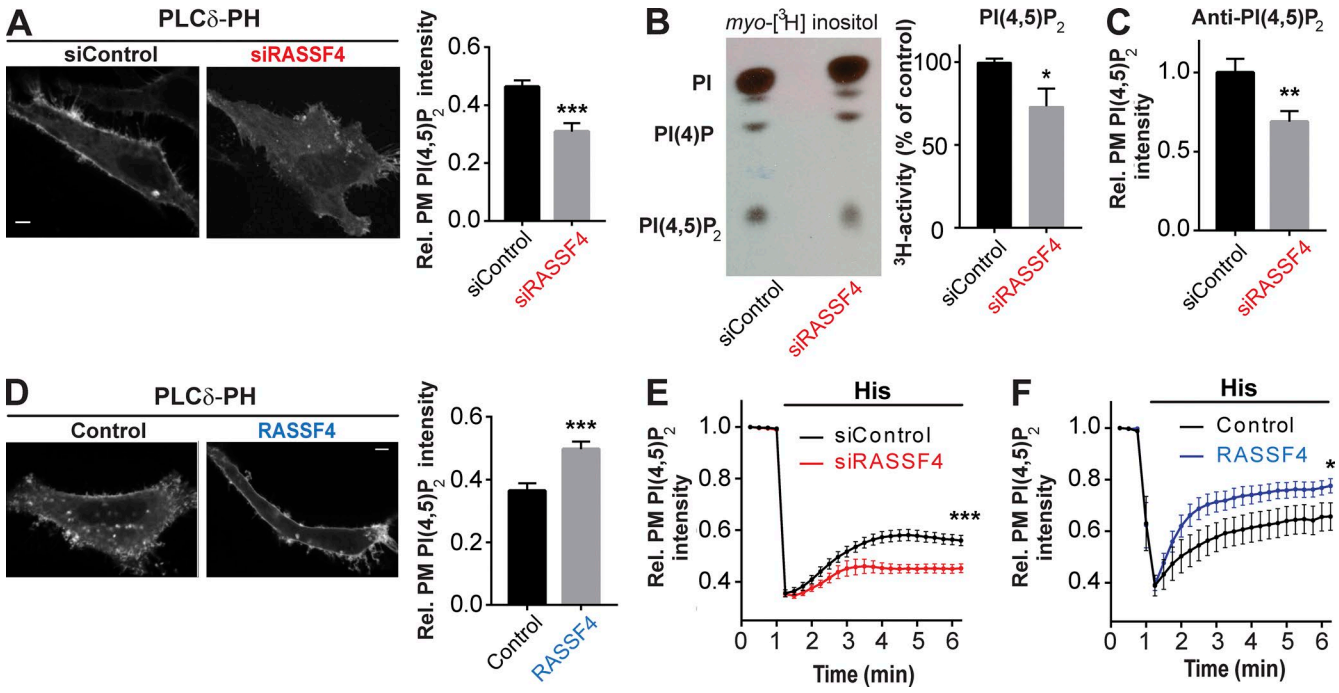

Figure 6. **RASSF4 regulates the levels of PI(4,5)P_2.** (A) Confocal images of HeLa cells expressing mCherry–PLCδ-PH and treated with either siRASSF4 or siControl. Bar, 5 µm. Relative (Rel.) mCherry–PLCδ-PH fluorescence intensity at the PM from >30 cells across three independent experiments was evaluated. Means ± SEM are shown. (B) Incorporation of myo-[^{3}H]inositol into phosphoinositides for 24 h in HeLa cells treated with either siControl or siRASSF4. Means ± SEM of four replicates from two independent experiments are shown. PI, phosphatidylinositol. (C) Relative PM PI(4,5)P_2 levels by anti-PI(4,5)P_2 staining were quantified from >30 cells across three independent experiments. Means ± SEM are shown. (D) Confocal images of HeLa cells cotransfected with mCherry–PLCδ-PH and either RASSF4-YFP or a control vector. Bar, 5 µm. Relative mCherry–PLCδ-PH fluorescence intensity in the PM from >30 cells across three independent experiments was evaluated. Means ± SEM are shown. (E) Changes in PM PI(4,5)P_2 levels induced by 100 µM histamine (His) monitored in HeLa cells cotransfected with H1R and GFP–PLCδ-PH together with either siControl (n = 19) or siRASSF4 (n = 12). Means ± SEM are shown. (F) Changes in PM PI(4,5)P_2 levels induced by 100 µM His monitored in HeLa cells cotransfected with H1R and GFP–PLCδ-PH together with either a control vector (n = 9) or RASSF4 (n = 14). Means ± SEM are shown. *, P < 0.05; **, P < 0.01; ***, P < 0.001.

different nucleotide-binding states, such as ARF6-T27N (GDP bound), ARF6-Q67L (GTP bound), and ARF6-N122I (nucleotide free), were used to determine the state in which ARF6 interacts with RASSF4. A preferential association of RASSF4 with ARF6-T27N and ARF6-N122I, but not ARF6-Q67L, was detected (Fig. 8 D). These results support the specificity of RASSF4–ARF6 interaction and suggest that RASSF4 regulates ARF6 activation by interacting with ARF6 in its GDP-bound and nucleotide-free states.

Our data suggest that ARF6, regulated by RASSF4, is involved in the regulation of SOCE. Consistent with this hypothesis, expression of the ARF6-N122I mutant, which has a dominant-negative effect on PM targeting of PIP5K1B (Honda et al., 1999), reduced SOCE in a fashion similar to siRASSF4 treatment (Fig. 8 E). Based on our findings, we propose that RASSF4 acts upstream of ARF6 to regulate the localization and activation of PIP5Ks and PI(4,5)P_2 production (Fig. 8 F). By affecting the PM PI(4,5)P_2 level, RASSF4 controls SOCE, ER–PM junctions, and other PI(4,5)P_2-dependent biological processes.

Discussion

In this study, we report that RASSF4 is a novel regulator of SOCE and ER–PM junctions. The expression level of RASSF4 controls the number and stability of ER–PM junctions in resting cells and the extent of SOCE in receptor-stimulated cells. By affecting steady-state PM PI(4,5)P_2 levels, RASSF4 regulates targeting of ER membrane proteins E-Syt2, E-Syt3, and STIM1 to ER–PM junctions. RASSF4 interacts with and regulates the localization and activation of ARF6, which can directly activate PIP5Ks and control the levels of PI(4,5)P_2. This study not only reveals new functions of RASSF4, but also provides insights into molecular mechanisms underlying these functions.

RASSF4 is 1 of 10 RASSF proteins implicated in tumorigenesis; yet, a role of RASSF proteins in SOCE had not been demonstrated previously. Diced pools of siRNAs designed to target each of the 10 RASSF proteins were included in the siRNA screen for SOCE regulators in HeLa cells (Liou et al., 2005). Only the siRNA pool targeting *RASSF4* had a significant effect on sustained Ca^{2+} responses. Among the 10 family members, RASSF1–RASSF6 contain the homologous RA and SARAH domains at the C terminus with divergent N terminal regions (Chan et al., 2013). Notably, in cells treated with siRASSF4_N' targeting the coding sequence of the distinct N-terminal region of RASSF4 protein, SOCE was suppressed to the same extent as that in cells treated with siRASSF4_C' (Fig. 1 C). Furthermore, similar suppression of SOCE was observed in siRASSF4-treated noncancerous HUVECs and RPE-1 cells (Fig. 1, D and E). These findings indicate that among RASSF proteins, RASSF4 is the major regulator of SOCE in these cells.

SOCE is mediated by STIM1 interaction with Orai1 at ER–PM junctions. Several additional SOCE regulators have been identified using siRNA screens or biochemical approaches since the discovery of STIM1 and Orai1. Many of these regulators, including CRACR2A, SARAF, Junctate, α-SNAP,

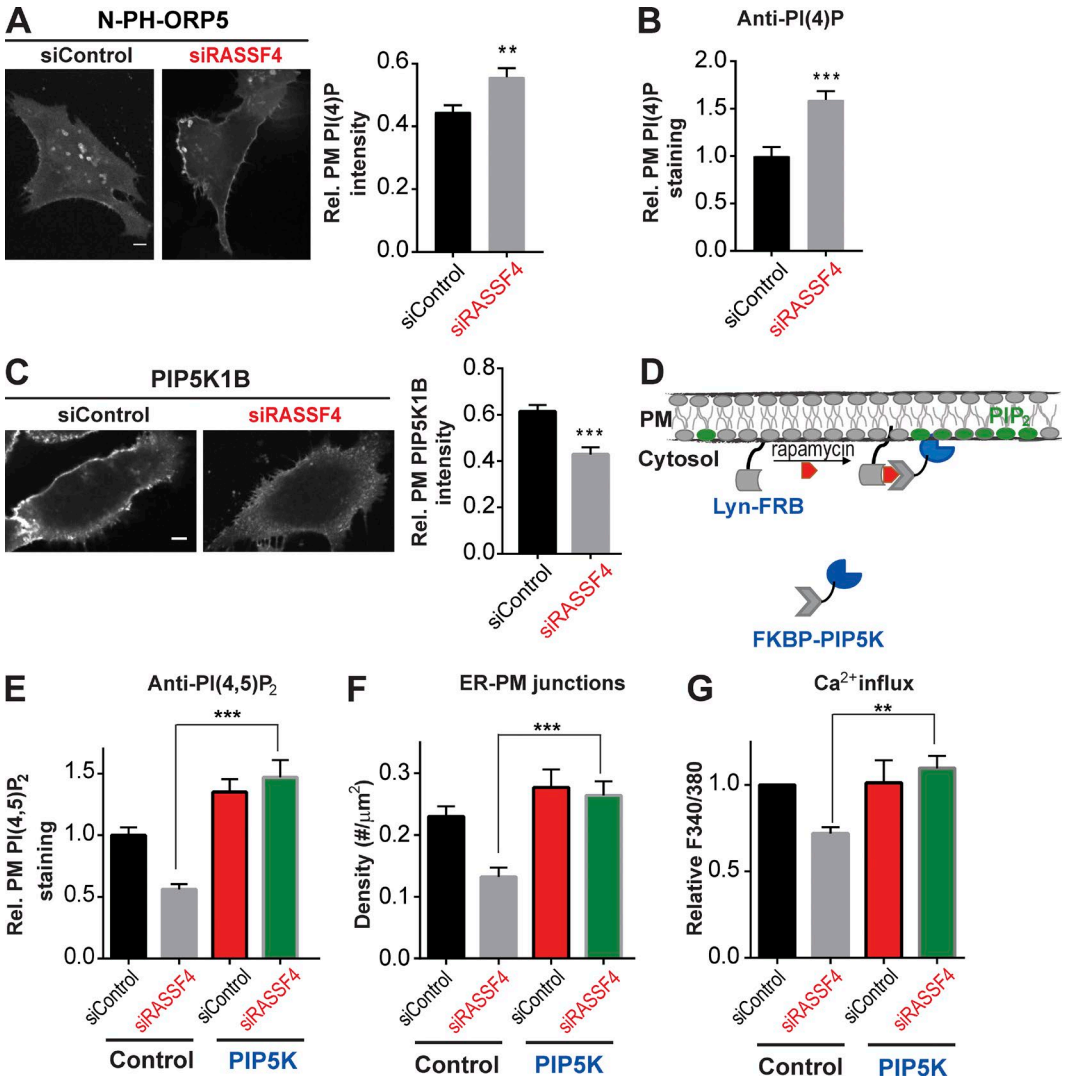

Figure 7. **RASSF4 regulates the levels of PI(4)P and PIP5Ks at the PM.** (A) Confocal images of HeLa cells expressing N-PH-ORP5-GFP and treated with either siControl of siRASSF4. Bar, 5 µm. Relative N-PH-ORP5-GFP fluorescence intensity in the PM from >30 cells across three independent experiments was evaluated. Means ± SEM are shown. (B) Relative PM PI(4)P levels were detected by anti-PI(4)P antibody in HeLa cells treated with either siControl or siRASSF4 from ~30 cells across three independent experiments. Means ± SEM are shown. (C) Confocal images of HeLa cells expressing YFP-PIP5K1B, treated with either siRASSF4 or siControl. Bar, 5 µm. Relative YFP-PIP5K1B fluorescence intensity in the PM from >30 cells across two independent experiments was evaluated. Means ± SEM are shown. (D) A diagram of the rapamycin-inducible approach that selectively increases $PI(4,5)P_2$ at the PM. (E) Relative PM $PI(4,5)P_2$ levels in HeLa cells transfected with the indicated siRNA, Lyn-FRB, and either CFP-FRBP-PIP5K or CFP-FRBP-PIP5Ki (control) were monitored by $PI(4,5)P_2$ immunostaining. More than 30 cells for each condition across three independent experiments were evaluated. Means ± SEM are plotted. (C–E) Cells were treated with 5 µM rapamycin for 10 min after the transfection and before the experiments. (F) The density of stable ER puncta in HeLa cells treated with the indicated siRNA and expressing YFP-KDEL, mCherry-KRAS-tail, Lyn-FRB, and either CFP-FRBP-PIP5K or CFP-FRBP-PIP5Ki. More than 15 cells for each condition across two independent experiments were analyzed. Plotted are means ± SEM. (G) HeLa cells were transfected with the indicated siRNA, Lyn-FRB, and either CFP-FRBP-PIP5K or CFP-FRBP-PIP5Ki. Cells were stimulated with 100 µM His, 1 µM TG, and 2 mM EGTA; 2 mM Ca^{2+} was added 6 min after stimulation. Mean peak values of Fura-2 ratio ± SEM of the Ca^{2+} add-back phase are plotted from >300 cells for each condition across three independent experiments. **, $P < 0.01$; ***, $P < 0.001$. Rel., relative.

STIMATE/TMEM110, and Junctophilin-4, modulate SOCE by binding to STIM1 and/or Orai1 (Srikanth et al., 2010, 2012; Palty et al., 2012; Miao et al., 2013; Jing et al., 2015; Quintana et al., 2015; Woo et al., 2016). Instead, RASSF4 regulates SOCE by affecting steady-state PM $PI(4,5)P_2$ levels. Our finding supports an important role of PM $PI(4,5)P_2$ in STIM1 targeting to ER–PM junctions and is consistent with the model in which STIM1 translocates to ER–PM junctions by binding to PM $PI(4,5)P_2$ and subsequently recruits Orai1 to ER–PM junctions after ER Ca^{2+} depletion (Liou et al., 2007; Prakriya and Lewis, 2015). In addition, we demonstrate that PM $PI(4,5)P_2$ is crucial for the formation and stability of steady-state ER–PM junctions using several assays for quantitation and tracking of ER–PM junctions. It is possible that some ER–PM junctions do not survive long enough to allow productive STIM1 interaction with Orai1 for SOCE activation in *RASSF4*-knockdown cells. Therefore, defective STIM1 targeting to ER–PM junctions in *RASSF4*-knockdown cells might be caused by insufficient PM $PI(4,5)P_2$ and unstable ER–PM junctions.

PM $PI(4,5)P_2$ is required for the ER–PM tethering function of E-Syts, and triple knockdown of *ESYT1*, *ESYT2*, and *ESYT3* results in a reduction in ER–PM junctions without disrupting the activation of SOCE in HeLa cells (Giordano et al., 2013; Idevall-Hagren et al., 2015). In contrast to E-Syt tri-

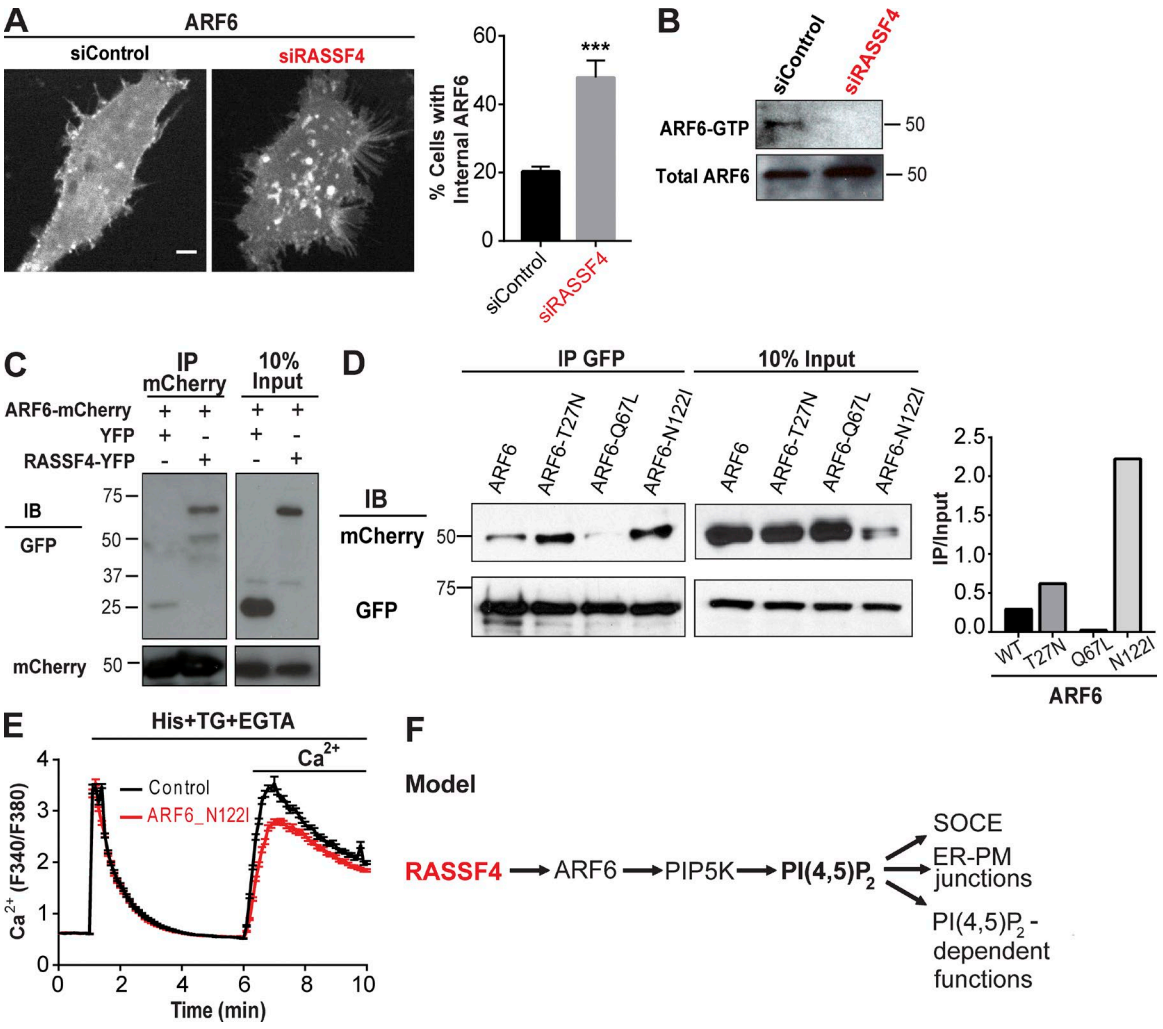

Figure 8. **RASSF4 interacts with ARF6 and regulates its localization and activation.** (A, left) Confocal images of HeLa cells expressing ARF6-mCherry, treated with either siRASSF4 or siControl. Bar, 5 µm. (Right) The percentage of cells with internal ARF6-mCherry aggregates was calculated from >400 cells across two independent experiments. Means ± SEM are shown. ***, $P < 0.001$. (B) ARF6 activity was measured in HeLa cells expressing ARF6-mCherry, treated with either siControl or siRASSF4. Anti-ARF6 and anti-mCherry antibodies were used to detect total ARF6-GTP and total ARF6, respectively, by immunoblotting. Total ARF6 was derived from 10% of input lysates. (C) Lysates from HeLa cells transfected with the indicated constructs were subjected to anti-mCherry immunoprecipitation (IP) and subsequent immunoblotting (IB) with anti-GFP and anti-mCherry. (D, left) Lysates of HeLa cells transfected with RASSF4-YFP and the indicated ARF6 construct were subjected to anti-GFP immunoprecipitation and subsequent immunoblotting with anti-GFP and anti-mCherry. (Right) Relative intensities (IP/Input) of ARF6 and its variants determined by ImageJ. (B–D) The unit of molecular weight shown next to immunoblots is kilodaltons. Similar results were obtained in more than three independent experiments. (E) Intracellular Ca^{2+} levels determined by analysis of Fura-2 fluorescence ratios in HeLa cells treated with ARF6-N122I or a control vector, stimulated with 1 µM TG and 100 µM histamine (His). 2 mM Ca^{2+} was added 6 min after stimulation. Shown are mean Fura-2 ratios ± SEM derived from >350 cells for each condition across two independent experiments. (F) Model of PM $PI(4,5)P_2$ regulation by RASSF4 through the ARF6-PIP5K pathway.

ple-knockdown cells, both SOCE and ER–PM junctions were disrupted in *RASSF4*-knockdown cells. Our data reveal that, by controlling steady-state PM $PI(4,5)P_2$ levels, RASSF4 has a dominant effect over the activation of STIM1 to regulate SOCE and the function of E-Syts to form ER–PM junctions. As PM $PI(4,5)P_2$ controls the localization and functions of numerous proteins in addition to STIM1 and E-Syts (Balla, 2013), it is expected that RASSF4 impacts a broad array of physiological processes, such as cell motility, vesicular trafficking, and cytoskeleton reorganization.

Aside from Ca^{2+} signaling, ER–PM junctions are important for nonvesicular lipid transport between the ER and the PM (Henne et al., 2015). The formation and stability of ER–PM junctions may affect the functions of lipid transfer proteins such as Nir2 and Nir3 that exchange phosphatidylinositol and phosphatidic acid at ER–PM junctions to support receptor-induced signaling and maintain PM $PI(4,5)P_2$ levels (Chang et al., 2013; Kim et al., 2013, 2015; Chang and Liou, 2015; Yadav et al., 2015). Consistently, the replenishment of PM $PI(4,5)P_2$ after receptor-induced hydrolysis was suppressed in *RASSF4*-knockdown cells and was promoted in RASSF4-overexpressing cells (Fig. 6, E and F). Thus, the defective replenishment of PM $PI(4,5)P_2$ in *RASSF4*-knockdown cells may result from decreased ER–PM junctions and reduced production of $PI(4,5)P_2$ from PI(4)P.

The accumulation of PM PI(4)P in *RASSF4*-knockdown cells may result from disrupted conversion of PI(4)P to $PI(4,5)P_2$ caused by defects in ARF6 activation and localization of PIP5Ks. Indeed, acute recruitment of an active PIP5K to the PM rescued the defects in PM $PI(4,5)P_2$ levels, SOCE, and ER–PM

junctions in *RASSF4*-knockdown cells (Fig. 7). In addition, reduction in ER–PM junctions in *RASSF4*-knockdown cells may contribute to the increase in PM PI(4)P by limiting transport of PI(4)P from the PM to the ER by oxysterol-binding protein–related protein 5 (ORP5) and ORP8 (Chung et al., 2015; Moser von Filseck et al., 2015) or by preventing Sac1-mediated dephosphorylation of PI(4)P to generate phosphatidylinositol at ER–PM junctions (Stefan et al., 2011; Dickson et al., 2016).

A role of RASSF proteins in regulating the levels of phosphoinositides had not been shown previously. Our data support a model in which RASSF4 regulates ARF6 activation, which directly activates PIP5Ks to affect PM PI(4,5)P_2 levels (Fig. 8 F). Several small G proteins, including ARF6, RhoA, and Rac1, have been reported to regulate the activity and localization of PIP5Ks (van den Bout and Divecha, 2009). Nevertheless, the activation of PIP5K by RhoA and Rac1 are likely to be indirect (Funakoshi et al., 2011). RASSF4 preferentially binds ARF6 in its GDP-bound and nucleotide-free states, suggesting that RASSF4 is involved in the nucleotide exchange process from ARF6-GDP to ARF6-GTP (Cherfils and Chardin, 1999). However, RASSF4 is not related to any known guanine nucleotide exchange factors of ARF6. Thus, it is of interest to investigate the mechanism by which RASSF4 affects the activation process of ARF6 and the upstream signaling pathways that regulate RASSF4.

Involvement of RASSF4 in cancer progression has been demonstrated by numerous studies (Chow et al., 2004; Crose et al., 2014; Han et al., 2016). In addition, RASSF4 has been shown to bind MST1 of the Hippo pathway (Crose et al., 2014). Here, we discover that RASSF4 regulates PM PI(4,5)P_2 via the ARF6/PIP5K pathway. Notably, RASSF4, ARF6, PIP5K, and the Hippo pathway are all linked to cancer development (van den Bout and Divecha, 2009; Harvey et al., 2013; Hashimoto et al., 2016; Yoo et al., 2016). Therefore, our new findings on RASSF4 open a field in studying the interactions among ARF6, phosphoinositide metabolism, Ca^{2+} signaling, ER–PM contact sites, and the Hippo pathway. These studies may advance our understanding of tumorigenesis associated with these pathways and help design new therapeutic strategies for treating human cancers.

Materials and methods

Reagents and antibodies

TG, pluronic F-127, and Fura-2 AM were purchased from Invitrogen. All chemicals for extracellular buffer (ECB; 125 mM NaCl, 5 mM KCl, 1.5 mM $MgCl_2$, 20 mM Hepes, 10 mM glucose, and 1.5 mM $CaCl_2$, pH 7.4), penicillin and streptomycin solutions, rapamycin, histamine, and EGTA were obtained from Sigma-Aldrich. siRNAs used in this study were generated as described previously (Liou et al., 2005). Primers used for siRNA generation are listed in Table S1. Monoclonal anti-PI(4,5)P_2 antibody (clone 2C11) and anti-PI(4)P antibody were obtained from Echelon Bioscience. Anti-RASSF4 antibody (C18182) was obtained from Assay Biotech. Anti-STIM1 antibody (4916) was obtained from Cell Signaling Technology. Anti-Orai1 antibody (PA1-74181) and anti-GAPDH antibody (MA5-15738) were obtained from Thermo Scientific. Anti-GFP antibody (ab290) was purchased from Abcam. Anti-mCherry antibody (632496) was purchased from Clontech. Protein standard (161-0373) and DNA ladder (SM1153) were purchased from Bio-Rad and Thermo Scientific, respectively.

Cell culture and transfection

HeLa cells purchased from American Type Culture Collection were cultured in minimum essential medium supplemented with 10% fetal bovine serum (HyClone) and 1× penicillin and streptomycin solution. 50 ng of DNA plasmids and 25 nM siRNAs were cotransfected into HeLa cells with TransIT-LT1 reagent (Mirus Bio) for DNA plasmids and TransIT-TKO reagent (Mirus Bio) for siRNAs. For experiments with NFAT-YFP, STIM1-CT, STIM1-D76A, MAPPER, PIP5K, or ARF6, sequential transfection of siRNA and DNA plasmids was performed using TransIT-TKO reagent for siRNAs and TransIT-X2 reagent (Mirus Bio) for DNA plasmids. HUVECs were obtained from T. Meyer (Stanford University, Stanford, CA) and cultured using the EGM-2 BulletKit (CC-3162; Lonza). Transfection of DNA plasmids and siRNAs into HUV ECs was done as described previously (Tsai and Meyer, 2012) using Lipofectamine 2000 (Invitrogen) for DNA plasmids and RNAiMAX (Invitrogen) for siRNAs. RPE-1 cells purchased from American Type Culture Collection were cultured in DMEM supplemented with 10% fetal bovine serum (HyClone) and 1× penicillin and streptomycin solution. siRNAs were transfected into RPE-1 cells with RNAiMAX (Invitrogen).

DNA constructs

Construction of mCherry-STIM1, mCherry-STIM1-D76A, YFP-KDEL (Lys-Asp-Glu-Leu; the ER marker), and MAPPER was described previously (Liou et al., 2005; Chang et al., 2013). RASSF4-YFP was constructed by replacing the Orai1 region of Orai1-YFP (Várnai et al., 2007) with the full-length coding region of human *RASSF4* (NCBI RefSeq accession no. NM_032023.3). mCherry-STIM1-CT was generated as previously described (Sharma et al., 2013). GFP–E-Syt3 and ARF6-mCherry were constructed using PCR and a human cDNA library. PIP5K1B-HA and PIP5K1C-HA were provided by H. Yin (University of Texas Southwestern Medical Center, Dallas, TX). YFP-PIP5K1B and YFP-PIP5K1C were constructed by inserting a PCR fragment of full-length PIP5K1B or PIP5K1C into a YFP-C1 vector. GFP-FKBP-PIP5K was constructed by replacing the CFP region of CFP-FKBP-PIP5K with GFP. Mutants of ARF6 were generated using a QuikChange site-directed mutagenesis kit (Agilent Technologies). All constructs were verified by sequencing. Oligonucleotides used in this study are listed in Table S1. The GFP–PLCδ-PH (Stauffer et al., 1998), CFP-FKBP-PIPK (Suh et al., 2006), CFP-FKBP-PIPKi (Suh et al., 2006), and Lyn-FRB (Inoue et al., 2005) DNA constructs were provided by T. Meyer (Stanford University, Stanford, CA). The GFP-PH-Osh2×2 (Balla et al., 2008) and Orai1-YFP (Varnai et al., 2007) DNA plasmids were provided by T. Balla (National Institutes of Health, Bethesda, MD). The N-PH-ORP5-GFP (Chung et al., 2015) and GFP–E-Syt2S (Giordano et al., 2013) DNA plasmids were gifts from P. De Camilli (Yale University, New Haven, CT). The HRP-ER (Wu et al., 2006) DNA plasmid was provided by R. Lewis (Stanford University, Stanford, CA). The Tubby-GFP (Quinn et al., 2008) DNA plasmid was a gift from A. Tinker (University College London, London, England, UK).

Ca^{2+} measurements

Cells were loaded with 0.5 µM Fura-2 AM, a Ca^{2+} indicator, in ECB containing 0.05% pluronic F-127 and 0.1% BSA for 30 min at room temperature. Then, Fura-2–loaded cells were washed twice with ECB containing 0.1% BSA and incubated in ECB for another 15–30 min before the experiments. Single-cell Fura-2 images were taken with a Plan Fluor 4×/0.15 objective on a microscope (Ti-E; Nikon) with a camera (HQ2; Photometrics). Intracellular Ca^{2+} levels were reported as the ratio of the fluorescence intensity at 510 nm excited at 340 nm over that excited at 380 nm (F340/F380). For Ca^{2+} add-back experiments, 100 µM histamine, 1 µM TG, and 2 mM EGTA were simultaneously added to cells to stimulate ER Ca^{2+} release while inhibiting ER Ca^{2+}

refill and chelating extracellular Ca^{2+}. After the ER Ca^{2+} store was depleted, 2 mM Ca^{2+} was added back to the ECB, enabling Ca^{2+} influx. For monitoring constitutive Ca^{2+} influx mediated by either STIM1-CT or STIM1-D76A, 2 mM EGTA was used to remove extracellular Ca^{2+}, and 2 mM Ca^{2+} was subsequently added back to reinitiate Ca^{2+} influx.

Mn^{2+} quench assays

Mn^{2+} influx–induced Fura-2 quenching was used to measure divalent cation influx, using Mn^{2+} as a surrogate for Ca^{2+} (Liou et al., 2005). Cells were loaded with 0.5 µM Fura-2 AM in ECB containing 0.05% pluronic F-127 and 0.1% BSA for 30 min at room temperature. Subsequently, cells were washed twice with ECB containing 0.1% BSA and incubated in ECB for another 15–30 min. Then, cells were incubated in Ca^{2+}-free ECB and treated with 1 µM TG for 5 min before the addition of 10 mM Mn^{2+}. Single-cell Fura-2 images were taken every 5 s with a Plan Fluor 4×/0.15 objective on a Ti-E microscope with an HQ2 camera. Excitation light was provided through a 360-nm filter, and an emission filter of 510 nm was applied to the light path. Quenching of Fura-2 fluorescence was reported as F/F0, where F is the fluorescence intensity recorded at each time, and F0 is the fluorescence intensity before the addition of Mn^{2+}.

NFAT nuclear translocation assay

HeLa cells were sequentially transfected with siRNA and NFAT-YFP plasmid as described in the Cell culture and transfection section. Cells were washed with ECB twice before imaging every 30 s at room temperature using a long working distance 20×/0.40 objective on a Ti-E microscope with an HQ2 camera. 1 µM TG was added to cells to trigger NFAT translocation from the cytosol to the nucleus. Images were analyzed using ImageJ software (National Institutes of Health). Nuclear translocation was assessed by calculating the ratio of the intensity of the nucleus to that of the whole cell. Cells with >50% of NFAT-YFP signal in the nucleus 10 min after TG treatment were scored as positive for nuclear translocation.

mRNA expression analysis

HeLa cells were lysed after treatment with siRNAs for 2 d, and total RNA was extracted using the RNeasy Mini kit (QIAGEN). cDNA was obtained by reverse transcription using a High-Capacity RNA-to-cDNA kit (Applied Biosystems). RT-PCR was performed using Phusion High-Fidelity DNA polymerase (New England Biolabs) and a Mastercycler pro S thermal cycler (Eppendorf). Products of RT-PCR were separated on agarose gels and quantitated by densitometry analysis (ImageJ). Oligonucleotides used in this study are listed in Table S1.

Live-cell confocal and TIRFM imaging

Cells were plated on 8-well Lab-Tek chambered cover glass (Nunc) at a low density the day before transfection. Transfected cells were washed with ECB and imaged in ECB at room temperature with a CFI Apo TIRF 60×/1.49 or a CFI Apo TIRF 100×/1.49 objective on a spinning-disc confocal and TIRF system built around a Ti-E Perfect Focus microscope (Nikon) with an HQ2 camera and an EM camera (c9100-13; Hamamatsu) controlled by Micro-Manager software (Edelstein et al., 2010). For mCherry-STIM1 translocation experiments, cells with low to moderate expression levels of mCherry-STIM1 were imaged near the adhesion surface using spinning-disc confocal microscopy or TIR FM. For TIRF imaging experiments, a PM marker was cotransfected into cells to monitor the focus and cell movements.

EM

EM and HRP-ER cytochemistry were performed as previously described (Wu et al., 2006). After transfection of the HRP-ER plasmid with either siRNAs or DNA plasmids, HeLa cells were plated onto coverslips (MatTek Corporation) and fixed with 2% glutaraldehyde (Electron Microscopy Sciences) in 0.1 M sodium cacodylate buffer (Electron Microscopy Sciences) for 20 min at room temperature. The HRP signals in fixed cells were amplified with a TSA Biotin system (PerkinElmer) and the ABC kit (Vector Laboratories) for 30 min each before the first reaction with 1 mg/ml DAB (Sigma-Aldrich) in Tris-buffered saline for 15 min and a subsequent reaction with DAB with 0.01% H_2O_2 for 30 min. DAB reaction was stopped by three sequential rinses with 0.1 M sodium cacodylate buffer. After postfixation with 1% OsO_4 and en bloc staining with 1% uranyl acetate, cells were further processed as previously described (Ahmari et al., 2000). After embedding in Embed 812 resin (Electron Microscopy Sciences), glass coverslips were removed. Cells were located using light microscopy and trimmed out. 60–70 nm–thin sections were cut, mounted on formvar-coated grids, and viewed by a transmission electron microscope (Tecnai G2 spirit; FEI) equipped with a LaB6 source using a voltage of 120 kV.

Analyses of PM occupancy by ER–PM junctions using EM

To measure lengths of HRP-ER–labeled ER tubules in close contact with the PM, micrographs with cells in which the nucleus was visible were selected. The total length of the PM and the length of HRP-positive ER segments making close contact with the PM (<50 nm) were measured. The percentage of PM occupancy by the ER was calculated as the sum of length of ER making contact with the PM divided by the length of the PM.

Quantitation of the density of ER–PM junctions using ER labeling

To determine the density of ER–PM junctions in a cell using ER labeling, TIRFM images of live cells expressing YFP-KDEL were taken every 15 s for 2.5 min. A time series of YFP-KDEL TIRFM images was summed, background subtracted, and subjected to Fourier transformation with a high-pass filter to create binary-like images that helped identify ER–PM junctions. The transformed images were subjected to threshold analysis to obtain the total number of ER–PM junctions. PM areas detected by a fluorescent protein–tagged PM marker (mCherry-KRAS-tail) were measured to obtain the density of ER–PM junctions (Fivaz and Meyer, 2005; Chang et al., 2013).

Analyses of the density of STIM1, MAPPER, and E-Syt2/3 puncta

To determine the density of STIM1, MAPPER, E-Syt2, or E-Syt3 puncta, TIRFM images of cells expressing mCherry-STIM1, MAP PER, GFP-E-Syt2, or GFP-E-Syt3 were background subtracted and subjected to Fourier transformation with a high-pass filter to create binary-like images. The transformed images were subjected to threshold analysis to obtain the total number of puncta. The density of puncta was obtained by dividing the total number of puncta by the PM areas detected using the PM marker mCherry-KRAS-tail.

Analyses of the stability of STIM1-D76A puncta and ER–PM junctions

TIRFM images of cells expressing mCherry-STIM1-D76A or MAP PER were taken every 15 s for 5 min. Stable puncta were determined using the following criteria: the area of puncta was >10 pixels and the location of puncta remained at the same position throughout the 20 frames of the 5-min image series. The percentage of stable puncta was calculated as the number of stable puncta in the image series multiplied by the number of image frames and divided by the sum of the number of puncta detected in all image frames.

Measurements of PM PI(4)P, PI(4,5)P_2, and PIP5K levels

PM PI(4)P, PI(4,5)P_2, and PIP5K levels were determined by analysis of the ratio of the intensity of N-PH-ORP5-GFP, GFP-PH-Osh2×2,

mCherry–PLCδ-PH, YFP-PIP5K1B, and YFP-PIP5K1C at the PM to that in the cytosol by line scan using confocal images as described previously (Stauffer et al., 1998). For direct measurements of PI(4)P and PI(4,5)P_2 using immunostaining, monoclonal anti-PI(4)P and anti-PI(4,5)P_2 antibody (clone 2C11), respectively, were used following a previously described protocol (Hammond et al., 2009). Cells plated on 8-well chamber cover glass were fixed with 4% formaldehyde and 0.2% glutaraldehyde in PBS for 15 min at room temperature. After fixation, cells were washed three times with PBS containing 50 mM NH_4Cl. Cells on cover glass were chilled on ice for at least 2 min. Then, cells were blocked and permeabilized for 45 min at 4°C with prechilled buffer A (20 mM Pipes, pH 6.8, 137 mM NaCl, and 2.7 mM KCl) containing 5% (vol/vol) normal goat serum (NGS), 50 mM NH_4Cl, and 0.5% saponin. Cells were rinsed twice with buffer A before incubation with primary antibodies (2.5 µg/ml for anti-PI[4,5]P_2 antibody and 8 µg/ml for anti-PI[4]P antibody) in buffer A with 5% NGS and 0.1% saponin for 1 h at 4°C. Cells were washed twice with buffer A before incubation with the secondary antibody (anti–mouse Alexa Fluor 488; 1:1,000 dilution) in buffer A with 5% NGS and 0.1% saponin at 4°C for 45 min. Cells were rinsed four times with buffer A, postfixed in 2% formaldehyde in PBS containing 50 mM NH_4Cl on ice for 10 min, and then incubated at room temperature for 5 min. Cells were rinsed once with distilled water and two more times with PBS. Cells were imaged using a spinning-disc confocal setup built around a Ti-E Perfect Focus microscope equipped with an EM camera (c9100-13). For measurement of dynamic changes in PM PI(4,5)P_2 levels induced by histamine stimulation, HeLa cells transfected with histamine H1 receptor (H1R) and GFP–PLCδ-PH DNA plasmids were imaged using a TIRF imaging system built around a Ti-E Perfect Focus microscope equipped with an HQ2 camera. Changes in PM PI(4,5)P_2 levels were determined by the ratio of the intensity of GFP–PLCδ-PH measured at each time point to that measured before the addition of histamine.

Analysis of myo-[^{3}H]inositol–labeled lipids

HeLa cells plated on 6-well plates were transfected with siRNAs and labeled with 20 µCi/ml myo-[^{3}H]inositol (PerkinElmer) in inositol-free DMEM supplemented with 5% dialyzed fetal bovine serum for 24 h. The labeling was terminated by the addition of a 250-µl mixture of methanol and 1 M hydrochloric acid (1:1 vol/vol). Then, cells were scraped and transferred into tubes, and 125 µl of chloroform was added to extract lipids. The samples were vortexed and centrifuged at 14,000 rpm for 1 min, and then, the phospholipids were separated by TLC in an n-propyl alcohol/H_2O/NH_4Cl (65:20:15) solvent system as described previously (Barylko et al., 2001). TLC plates were sprayed with autoradiography enhancer (KODAK) and then exposed to x-ray films. Radioactive PI(4,5)P_2 levels were quantified by densitometry analysis (Image J).

ARF6 activation assay

ARF6 activity was measured using an ARF6 Pull-Down Activation Assay Biochem kit (BK033-S; Cytoskeleton) according to the manufacturer's instructions. In brief, ARF6-mCherry–transfected cells were lysed on ice for 10 min with cell lysis buffer (25 mM Tris, pH 7.2, 5 mM $MgCl_2$, 150 mM NaCl, 1% IGEPAL, and 1× protease inhibitor cocktail). Lysates were clarified by centrifugation at 10,000 *g* for 2 min. Cell lysates were incubated with GGA3 beads for 1–2 h at 4°C. Then, the beads were washed three times with wash buffer (25 mM Tris, pH 7.5, 30 mM $MgCl_2$, and 40 mM NaCl). Proteins bound to the beads were eluted into 2× sample buffer, separated by SDS-PAGE, and subjected to immunoblotting using anti-mCherry antibody and anti-ARF6 antibody. Chemiluminescence detection of immunoblotting was performed using SuperSignal West Dura Extended Duration substrate (34076; Thermo Scientific).

Immunoprecipitation

For immunoprecipitation of YFP-tagged or mCherry-tagged protein, transfected cells were collected and lysed in NP-40 lysis buffer (50 mM Tris, pH 7.7, 150 mM NaCl, 0.5% NP-40, 1 mM dithiothreitol, and 1× protease inhibitor cocktail) on ice for 20 min. Then, cell lysates were centrifuged at 4°C and 16,000 *g* for 10 min, and supernatants were incubated with Chromotek GFP-trap or RFP-trap magnetic beads (Allele Biotech) at 4°C for 16 h. Immunoprecipitated proteins were eluted with 2× sample buffer (Bio-Rad) after washing the beads five times with wash buffer (10 mM Tris, pH 7.5, and 150 mM NaCl) and analyzed by immunoblotting using antibodies against GFP or mCherry.

Statistical analysis

Unpaired Student's *t* test was used for statistical analysis. A p-value < 0.05 was considered statistically significant.

Online supplemental material

Fig. S1 shows Ca^{2+} traces demonstrating that RASSF4-YFP expression rescued SOCE in siRASSF4-treated cells, and results, similar to those in HeLa cells, were obtained in RPE-1 cells. It also shows immunoblots and RT-PCR results demonstrating that expression levels of STIM1 and Orai1 proteins, as well as several other genes implicated in regulating SOCE, were not affected in siRASSF4-treated cells. Fig. S2 shows quantitation of MAPPER-labeled ER–PM junctions demonstrating reduction in ER–PM junctions in *RASSF4*-knockdown cells. Fig. S3 shows confocal images of HeLa cells transfected with Tubby-GFP, GFP-PH-Osh2×2, or YFP-PIP5K1C and treated with either siControl or siRASSF4 demonstrating that RASSF4 regulates PM PI(4,5)P_2, PI(4)P, and PIP5K levels. Fig. S4 shows confocal images of HeLa cells demonstrating rapamycin-induced PM targeting of FKBP-PIP5K and FKBP-PIP5Ki and shows quantitation of MAPPER-labeled ER–PM junctions and STIM1 puncta demonstrating reconstitution of ER–PM junctions and TG-triggered STIM1 translocation in *RASSF4*-knockdown cells by PM targeting of PIP5K. Fig. S5 shows confocal images of HeLa cells demonstrating the diffuse distribution of RASSF4-YFP in the cytoplasm. Video 1 is a time-lapse video demonstrating RASSF4 regulates mCherry-STIM1 translocation to ER–PM junctions during SOCE in live HeLa cells. Table S1 is available as an Excel file and shows oligonucleotides used in this study.

Acknowledgments

We thank Dr. Sandra Schmid for her kind reading and suggestions on this manuscript. We appreciate Carlo Quintanilla for carefully reading this manuscript. We thank Drs. Joseph Albanesi and Barbara Barylko for assistance in the [^{3}H]inositol labeling experiment and the University of Texas Southwestern Live-Cell Imaging Facility for assistance with EM. We thank Drs. Youxing Jiang and Yeeling Lam for assistance in protein purification necessary for this research. We are grateful to Drs. Tobias Meyer, Helen Yin, Tamas Balla, Pietro De Camilli, Richard Lewis, and Andrew Tinker for providing reagents. We also thank the Liou laboratory members for valuable discussions and technical assistance. We are grateful to Linda Patterson and Carrie Ann Brown for administrative assistance.

This work was supported by National Institutes of Health grant GM113079 and Welch Foundation grant I-1789. Y.-J. Chen was supported by Taiwan National Science Council grant 102-2917-I-564-019. J. Liou is a Sowell Family Scholar in Medical Research.

The authors declare no competing financial interests.

Author contributions: Y.-J. Chen designed and performed all experiments except those indicated below. C.-L. Chang performed the experiments and analyzed the data shown in Figs. 1 C and 2

B. C.-L. Chang also generated the GFP-E-Syt3 plasmid. W.-R. Lee performed the experiments shown in Fig. S1 E. J. Liou conceived and supervised the project. J. Liou and Y.-J. Chen wrote the manuscript.

Submitted: 8 June 2016
Revised: 18 October 2016
Accepted: 27 April 2017

References

Ahmari, S.E., J. Buchanan, and S.J. Smith. 2000. Assembly of presynaptic active zones from cytoplasmic transport packets. *Nat. Neurosci.* 3:445–451. http://dx.doi.org/10.1038/74814

Balla, T. 2013. Phosphoinositides: tiny lipids with giant impact on cell regulation. *Physiol. Rev.* 93:1019–1137. http://dx.doi.org/10.1152/physrev.00028.2012

Balla, A., Y.J. Kim, P. Varnai, Z. Szentpetery, Z. Knight, K.M. Shokat, and T. Balla. 2008. Maintenance of hormone-sensitive phosphoinositide pools in the plasma membrane requires phosphatidylinositol 4-kinase IIIα. *Mol. Biol. Cell.* 19:711–721. http://dx.doi.org/10.1091/mbc.E07-07-0713

Barylko, B., S.H. Gerber, D.D. Binns, N. Grichine, M. Khvotchev, T.C. Südhof, and J.P. Albanesi. 2001. A novel family of phosphatidylinositol 4-kinases conserved from yeast to humans. *J. Biol. Chem.* 276:7705–7708. http://dx.doi.org/10.1074/jbc.C000861200

Bergmeier, W., C. Weidinger, I. Zee, and S. Feske. 2013. Emerging roles of store-operated Ca^{2+} entry through STIM and ORAI proteins in immunity, hemostasis and cancer. *Channels (Austin).* 7:379–391. http://dx.doi.org/10.4161/chan.24302

Brown, F.D., A.L. Rozelle, H.L. Yin, T. Balla, and J.G. Donaldson. 2001. Phosphatidylinositol 4,5-bisphosphate and Arf6-regulated membrane traffic. *J. Cell Biol.* 154:1007–1018. http://dx.doi.org/10.1083/jcb.200103107

Bunney, T.D., and M. Katan. 2010. Phosphoinositide signalling in cancer: beyond PI3K and PTEN. *Nat. Rev. Cancer.* 10:342–352. http://dx.doi.org/10.1038/nrc2842

Chan, J.J., D. Flatters, F. Rodrigues-Lima, J. Yan, K. Thalassinos, and M. Katan. 2013. Comparative analysis of interactions of RASSF1-10. *Adv. Biol. Regul.* 53:190–201. http://dx.doi.org/10.1016/j.jbior.2012.12.001

Chang, C.L., and J. Liou. 2015. Phosphatidylinositol 4,5-bisphosphate homeostasis regulated by Nir2 and Nir3 proteins at endoplasmic reticulum-plasma membrane junctions. *J. Biol. Chem.* 290:14289–14301. http://dx.doi.org/10.1074/jbc.M114.621375

Chang, C.L., and J. Liou. 2016. Homeostatic regulation of the $PI(4,5)P_2$–Ca^{2+} signaling system at ER–PM junctions. *Biochim. Biophys. Acta.* 1861:862–873. http://dx.doi.org/10.1016/j.bbalip.2016.02.015

Chang, C.L., T.S. Hsieh, T.T. Yang, K.G. Rothberg, D.B. Azizoglu, E. Volk, J.C. Liao, and J. Liou. 2013. Feedback regulation of receptor-induced Ca^{2+} signaling mediated by E-Syt1 and Nir2 at endoplasmic reticulum-plasma membrane junctions. *Cell Reports.* 5:813–825. http://dx.doi.org/10.1016/j.celrep.2013.09.038

Cherfils, J., and P. Chardin. 1999. GEFs: structural basis for their activation of small GTP-binding proteins. *Trends Biochem. Sci.* 24:306–311. http://dx.doi.org/10.1016/S0968-0004(99)01429-2

Chow, L.S., K.W. Lo, J. Kwong, A.Y. Wong, and D.P. Huang. 2004. Aberrant methylation of RASSF4/AD037 in nasopharyngeal carcinoma. *Oncol. Rep.* 12:781–787.

Chung, J., F. Torta, K. Masai, L. Lucast, H. Czapla, L.B. Tanner, P. Narayanaswamy, M.R. Wenk, F. Nakatsu, and P. De Camilli. 2015. PI4P/phosphatidylserine countertransport at ORP5- and ORP8-mediated ER-plasma membrane contacts. *Science.* 349:428–432. http://dx.doi.org/10.1126/science.aab1370

Crose, L.E., K.A. Galindo, J.G. Kephart, C. Chen, J. Fitamant, N. Bardeesy, R.C. Bentley, R.L. Galindo, J.T. Chi, and C.M. Linardic. 2014. Alveolar rhabdomyosarcoma-associated PAX3-FOXO1 promotes tumorigenesis via Hippo pathway suppression. *J. Clin. Invest.* 124:285–296. http://dx.doi.org/10.1172/JCI67087

Dickson, E.J., J.B. Jensen, O. Vivas, M. Kruse, A.E. Traynor-Kaplan, and B. Hille. 2016. Dynamic formation of ER–PM junctions presents a lipid phosphatase to regulate phosphoinositides. *J. Cell Biol.* 213:33–48. http://dx.doi.org/10.1083/jcb.201508106

Dittfeld, C., A.M. Richter, K. Steinmann, A. Klagge-Ulonska, and R.H. Dammann. 2012. The SARAH domain of RASSF1A and its tumor suppressor function. *Mol. Biol. Int.* 2012:196715. http://dx.doi.org/10.1155/2012/196715

Donaldson, J.G., and A. Honda. 2005. Localization and function of Arf family GTPases. *Biochem. Soc. Trans.* 33:639–642. http://dx.doi.org/10.1042/BST0330639

Edelstein, A., N. Amodaj, K. Hoover, R. Vale, and N. Stuurman. 2010. Computer control of microscopes using μManager. *Curr. Protoc. Mol. Biol.* Chapter 14:20.

Feske, S., Y. Gwack, M. Prakriya, S. Srikanth, S.H. Puppel, B. Tanasa, P.G. Hogan, R.S. Lewis, M. Daly, and A. Rao. 2006. A mutation in Orai1 causes immune deficiency by abrogating CRAC channel function. *Nature.* 441:179–185. http://dx.doi.org/10.1038/nature04702

Fivaz, M., and T. Meyer. 2005. Reversible intracellular translocation of KRas but not HRas in hippocampal neurons regulated by Ca^{2+}/calmodulin. *J. Cell Biol.* 170:429–441. http://dx.doi.org/10.1083/jcb.200409157

Funakoshi, Y., H. Hasegawa, and Y. Kanaho. 2011. Regulation of PIP5K activity by Arf6 and its physiological significance. *J. Cell. Physiol.* 226:888–895. http://dx.doi.org/10.1002/jcp.22482

Giordano, F., Y. Saheki, O. Idevall-Hagren, S.F. Colombo, M. Pirruccello, I. Milosevic, E.O. Gracheva, S.N. Bagriantsev, N. Borgese, and P. De Camilli. 2013. $PI(4,5)P_2$-dependent and Ca^{2+}-regulated ER-PM interactions mediated by the extended synaptotagmins. *Cell.* 153:1494–1509. http://dx.doi.org/10.1016/j.cell.2013.05.026

Hammond, G.R., G. Schiavo, and R.F. Irvine. 2009. Immunocytochemical techniques reveal multiple, distinct cellular pools of PtdIns4*P* and $PtdIns(4,5)P_2$. *Biochem. J.* 422:23–35. http://dx.doi.org/10.1042/BJ20090428

Han, Y., Q. Dong, J. Hao, L. Fu, X. Han, X. Zheng, and E. Wang. 2016. RASSF4 is downregulated in nonsmall cell lung cancer and inhibits cancer cell proliferation and invasion. *Tumour Biol.* 37:4865–4871. http://dx.doi.org/10.1007/s13277-015-4343-9

Harvey, K.F., X. Zhang, and D.M. Thomas. 2013. The Hippo pathway and human cancer. *Nat. Rev. Cancer.* 13:246–257. http://dx.doi.org/10.1038/nrc3458

Hashimoto, A., T. Oikawa, S. Hashimoto, H. Sugino, A. Yoshikawa, Y. Otsuka, H. Handa, Y. Onodera, J.M. Nam, C. Oneyama, et al. 2016. P53- and mevalonate pathway-driven malignancies require Arf6 for metastasis and drug resistance. *J. Cell Biol.* 213:81–95. http://dx.doi.org/10.1083/jcb.201510002

Henne, W.M., J. Liou, and S.D. Emr. 2015. Molecular mechanisms of inter-organelle ER–PM contact sites. *Curr. Opin. Cell Biol.* 35:123–130. http://dx.doi.org/10.1016/j.ceb.2015.05.001

Hogan, P.G., L. Chen, J. Nardone, and A. Rao. 2003. Transcriptional regulation by calcium, calcineurin, and NFAT. *Genes Dev.* 17:2205–2232. http://dx.doi.org/10.1101/gad.1102703

Honda, A., M. Nogami, T. Yokozeki, M. Yamazaki, H. Nakamura, H. Watanabe, K. Kawamoto, K. Nakayama, A.J. Morris, M.A. Frohman, and Y. Kanaho. 1999. Phosphatidylinositol 4-phosphate 5-kinase α is a downstream effector of the small G protein ARF6 in membrane ruffle formation. *Cell.* 99:521–532. http://dx.doi.org/10.1016/S0092-8674(00)81540-8

Idevall-Hagren, O., A. Lü, B. Xie, and P. De Camilli. 2015. Triggered Ca^{2+} influx is required for extended synaptotagmin 1-induced ER-plasma membrane tethering. *EMBO J.* 34:2291–2305. http://dx.doi.org/10.15252/embj.201591565

Jing, J., L. He, A. Sun, A. Quintana, Y. Ding, G. Ma, P. Tan, X. Liang, X. Zheng, L. Chen, et al. 2015. Proteomic mapping of ER–PM junctions identifies STIMATE as a regulator of Ca^{2+} influx. *Nat. Cell Biol.* 17:1339–1347. http://dx.doi.org/10.1038/ncb3234

Kim, S., A. Kedan, M. Marom, N. Gavert, O. Keinan, M. Selitrennik, O. Laufman, and S. Lev. 2013. The phosphatidylinositol-transfer protein Nir2 binds phosphatidic acid and positively regulates phosphoinositide signalling. *EMBO Rep.* 14:891–899. http://dx.doi.org/10.1038/embor.2013.113

Kim, Y.J., M.L. Guzman-Hernandez, E. Wisniewski, and T. Balla. 2015. Phosphatidylinositol-phosphatidic acid exchange by Nir2 at ER-PM contact sites maintains phosphoinositide signaling competence. *Dev. Cell.* 33:549–561. http://dx.doi.org/10.1016/j.devcel.2015.04.028

Liou, J., M.L. Kim, W.D. Heo, J.T. Jones, J.W. Myers, J.E. Ferrell Jr., and T. Meyer. 2005. STIM is a Ca^{2+} sensor essential for Ca^{2+}-store-depletion-triggered Ca^{2+} influx. *Curr. Biol.* 15:1235–1241. http://dx.doi.org/10.1016/j.cub.2005.05.055

Liou, J., M. Fivaz, T. Inoue, and T. Meyer. 2007. Live-cell imaging reveals sequential oligomerization and local plasma membrane targeting of stromal interaction molecule 1 after Ca^{2+} store depletion. *Proc. Natl. Acad. Sci. USA.* 104:9301–9306. http://dx.doi.org/10.1073/pnas.0702866104

Luik, R.M., M.M. Wu, J. Buchanan, and R.S. Lewis. 2006. The elementary unit of store-operated Ca^{2+} entry: local activation of CRAC channels by STIM1 at ER–plasma membrane junctions. *J. Cell Biol.* 174:815–825. http://dx.doi.org/10.1083/jcb.200604015

Makbul, C., D. Constantinescu Aruxandei, E. Hofmann, D. Schwarz, E. Wolf, and C. Herrmann. 2013. Structural and thermodynamic characterization

of Nore1-SARAH: a small, helical module important in signal transduction networks. *Biochemistry.* 52:1045–1054. http://dx.doi.org/10.1021/bi3014642

Maus, M., A. Jairaman, P.B. Stathopulos, M. Muik, M. Fahrner, C. Weidinger, M. Benson, S. Fuchs, S. Ehl, C. Romanin, et al. 2015. Missense mutation in immunodeficient patients shows the multifunctional roles of coiled-coil domain 3 (CC3) in STIM1 activation. *Proc. Natl. Acad. Sci. USA.* 112:6206–6211. http://dx.doi.org/10.1073/pnas.1418852112

Miao, Y., C. Miner, L. Zhang, P.I. Hanson, A. Dani, and M. Vig. 2013. An essential and NSF independent role for α-SNAP in store-operated calcium entry. *eLife.* 2:e00802. http://dx.doi.org/10.7554/eLife.00802

Moser von Filseck, J., A. Čopič, V. Delfosse, S. Vanni, C.L. Jackson, W. Bourguet, and G. Drin. 2015. Phosphatidylserine transport by ORP/Osh proteins is driven by phosphatidylinositol 4-phosphate. *Science.* 349:432–436. http://dx.doi.org/10.1126/science.aab1346

Padrón, D., Y.J. Wang, M. Yamamoto, H. Yin, and M.G. Roth. 2003. Phosphatidylinositol phosphate 5-kinase Iβ recruits AP-2 to the plasma membrane and regulates rates of constitutive endocytosis. *J. Cell Biol.* 162:693–701. http://dx.doi.org/10.1083/jcb.200302051

Palty, R., A. Raveh, I. Kaminsky, R. Meller, and E. Reuveny. 2012. SARAF inactivates the store operated calcium entry machinery to prevent excess calcium refilling. *Cell.* 149:425–438. http://dx.doi.org/10.1016/j.cell.2012.01.055

Peters, P.J., V.W. Hsu, C.E. Ooi, D. Finazzi, S.B. Teal, V. Oorschot, J.G. Donaldson, and R.D. Klausner. 1995. Overexpression of wild-type and mutant ARF1 and ARF6: distinct perturbations of nonoverlapping membrane compartments. *J. Cell Biol.* 128:1003–1017. http://dx.doi.org/10.1083/jcb.128.6.1003

Prakriya, M., and R.S. Lewis. 2015. Store-operated calcium channels. *Physiol. Rev.* 95:1383–1436. http://dx.doi.org/10.1152/physrev.00020.2014

Quinn, K.V., P. Behe, and A. Tinker. 2008. Monitoring changes in membrane phosphatidylinositol 4,5-bisphosphate in living cells using a domain from the transcription factor tubby. *J. Physiol.* 586:2855–2871. http://dx.doi.org/10.1113/jphysiol.2008.153791

Quintana, A., V. Rajanikanth, S. Farber-Katz, A. Gudlur, C. Zhang, J. Jing, Y. Zhou, A. Rao, and P.G. Hogan. 2015. TMEM110 regulates the maintenance and remodeling of mammalian ER-plasma membrane junctions competent for STIM-ORAI signaling. *Proc. Natl. Acad. Sci. USA.* 112:E7083–E7092.

Roos, J., P.J. DiGregorio, A.V. Yeromin, K. Ohlsen, M. Lioudyno, S. Zhang, O. Safrina, J.A. Kozak, S.L. Wagner, M.D. Cahalan, et al. 2005. STIM1, an essential and conserved component of store-operated Ca^{2+} channel function. *J. Cell Biol.* 169:435–445. http://dx.doi.org/10.1083/jcb.200502019

Roth, M.G. 2004. Phosphoinositides in constitutive membrane traffic. *Physiol. Rev.* 84:699–730. http://dx.doi.org/10.1152/physrev.00033.2003

Roy, A., and T.P. Levine. 2004. Multiple pools of phosphatidylinositol 4-phosphate detected using the pleckstrin homology domain of Osh2p. *J. Biol. Chem.* 279:44683–44689. http://dx.doi.org/10.1074/jbc.M401583200

Scheel, H., and K. Hofmann. 2003. A novel interaction motif, SARAH, connects three classes of tumor suppressor. *Curr. Biol.* 13:R899–R900. http://dx.doi.org/10.1016/j.cub.2003.11.007

Sharma, S., A. Quintana, G.M. Findlay, M. Mettlen, B. Baust, M. Jain, R. Nilsson, A. Rao, and P.G. Hogan. 2013. An siRNA screen for NFAT activation identifies septins as coordinators of store-operated Ca^{2+} entry. *Nature.* 499:238–242. http://dx.doi.org/10.1038/nature12229

Sherwood, V., A. Recino, A. Jeffries, A. Ward, and A.D. Chalmers. 2010. The N-terminal RASSF family: a new group of Ras-association-domain-containing proteins, with emerging links to cancer formation. *Biochem. J.* 425:303–311. http://dx.doi.org/10.1042/BJ20091318

Srikanth, S., H.J. Jung, K.D. Kim, P. Souda, J. Whitelegge, and Y. Gwack. 2010. A novel EF-hand protein, CRACR2A, is a cytosolic Ca^{2+} sensor that stabilizes CRAC channels in T cells. *Nat. Cell Biol.* 12:436–446. http://dx.doi.org/10.1038/ncb2045

Srikanth, S., M. Jew, K.D. Kim, M.K. Yee, J. Abramson, and Y. Gwack. 2012. Junctate is a Ca^{2+}-sensing structural component of Orai1 and stromal interaction molecule 1 (STIM1). *Proc. Natl. Acad. Sci. USA.* 109:8682–8687. http://dx.doi.org/10.1073/pnas.1200667109

Staiano, L., M.G. De Leo, M. Persico, and M.A. De Matteis. 2015. Mendelian disorders of PI metabolizing enzymes. *Biochim. Biophys. Acta.* 1851:867–881. http://dx.doi.org/10.1016/j.bbalip.2014.12.001

Stauffer, T.P., S. Ahn, and T. Meyer. 1998. Receptor-induced transient reduction in plasma membrane PtdIns(4,5)P_2 concentration monitored in living cells. *Curr. Biol.* 8:343–346. http://dx.doi.org/10.1016/S0960-9822(98)70135-6

Stefan, C.J., A.G. Manford, D. Baird, J. Yamada-Hanff, Y. Mao, and S.D. Emr. 2011. Osh proteins regulate phosphoinositide metabolism at ER-plasma membrane contact sites. *Cell.* 144:389–401. http://dx.doi.org/10.1016/j.cell.2010.12.034

Steinmann, K., A. Sandner, U. Schagdarsurengin, and R.H. Dammann. 2009. Frequent promoter hypermethylation of tumor-related genes in head and neck squamous cell carcinoma. *Oncol. Rep.* 22:1519–1526.

Steyer, J.A., and W. Almers. 2001. A real-time view of life within 100 nm of the plasma membrane. *Nat. Rev. Mol. Cell Biol.* 2:268–275. http://dx.doi.org/10.1038/35067069

Suh, B.C., T. Inoue, T. Meyer, and B. Hille. 2006. Rapid chemically induced changes of PtdIns(4,5)P_2 gate KCNQ ion channels. *Science.* 314:1454–1457. http://dx.doi.org/10.1126/science.1131163

Tsai, F.C., and T. Meyer. 2012. Ca^{2+} pulses control local cycles of lamellipodia retraction and adhesion along the front of migrating cells. *Curr. Biol.* 22:837–842. http://dx.doi.org/10.1016/j.cub.2012.03.037

van den Bout, I., and N. Divecha. 2009. PIP5K-driven PtdIns(4,5)P_2 synthesis: regulation and cellular functions. *J. Cell Sci.* 122:3837–3850. http://dx.doi.org/10.1242/jcs.056127

Várnai, P., B. Tóth, D.J. Tóth, L. Hunyady, and T. Balla. 2007. Visualization and manipulation of plasma membrane-endoplasmic reticulum contact sites indicates the presence of additional molecular components within the STIM1-Orai1 complex. *J. Biol. Chem.* 282:29678–29690. http://dx.doi.org/10.1074/jbc.M704339200

Vig, M., C. Peinelt, A. Beck, D.L. Koomoa, D. Rabah, M. Koblan-Huberson, S. Kraft, H. Turner, A. Fleig, R. Penner, and J.P. Kinet. 2006. CRACM1 is a plasma membrane protein essential for store-operated Ca^{2+} entry. *Science.* 312:1220–1223. http://dx.doi.org/10.1126/science.1127883

Walsh, C.M., M. Chvanov, L.P. Haynes, O.H. Petersen, A.V. Tepikin, and R.D. Burgoyne. 2010. Role of phosphoinositides in STIM1 dynamics and store-operated calcium entry. *Biochem. J.* 425:159–168. http://dx.doi.org/10.1042/BJ20090884

Wang, Y.J., W.H. Li, J. Wang, K. Xu, P. Dong, X. Luo, and H.L. Yin. 2004. Critical role of PIP5KIγ87 in $InsP_3$-mediated Ca^{2+} signaling. *J. Cell Biol.* 167:1005–1010. http://dx.doi.org/10.1083/jcb.200408008

Wong, K.W., and R.R. Isberg. 2003. Arf6 and phosphoinositol-4-phosphate-5-kinase activities permit bypass of the Rac1 requirement for β1 integrin–mediated bacterial uptake. *J. Exp. Med.* 198:603–614. http://dx.doi.org/10.1084/jem.20021363

Woo, J.S., S. Srikanth, M. Nishi, P. Ping, H. Takeshima, and Y. Gwack. 2016. Junctophilin-4, a component of the endoplasmic reticulum–plasma membrane junctions, regulates Ca^{2+} dynamics in T cells. *Proc. Natl. Acad. Sci. USA.* 113:2762–2767. http://dx.doi.org/10.1073/pnas.1524229113

Wu, M.M., J. Buchanan, R.M. Luik, and R.S. Lewis. 2006. Ca^{2+} store depletion causes STIM1 to accumulate in ER regions closely associated with the plasma membrane. *J. Cell Biol.* 174:803–813. http://dx.doi.org/10.1083/jcb.200604014

Yadav, S., K. Garner, P. Georgiev, M. Li, E. Gomez-Espinosa, A. Panda, S. Mathre, H. Okkenhaug, S. Cockcroft, and P. Raghu. 2015. RDGBα, a PtdIns-PtdOH transfer protein, regulates G-protein-coupled PtdIns(4,5)P_2 signalling during *Drosophila* phototransduction. *J. Cell Sci.* 128:3330–3344. http://dx.doi.org/10.1242/jcs.173476

Yoo, J.H., D.S. Shi, A.H. Grossmann, L.K. Sorensen, Z. Tong, T.M. Mleynek, A. Rogers, W. Zhu, J.R. Richards, J.M. Winter, et al. 2016. ARF6 is an actionable node that orchestrates oncogenic GNAQ signaling in uveal melanoma. *Cancer Cell.* 29:889–904. http://dx.doi.org/10.1016/j.ccell.2016.04.015

Zhang, S.L., A.V. Yeromin, X.H. Zhang, Y. Yu, O. Safrina, A. Penna, J. Roos, K.A. Stauderman, and M.D. Cahalan. 2006. Genome-wide RNAi screen of Ca^{2+} influx identifies genes that regulate Ca^{2+} release-activated Ca^{2+} channel activity. *Proc. Natl. Acad. Sci. USA.* 103:9357–9362. http://dx.doi.org/10.1073/pnas.0603161103

Zhou, Y., P. Srinivasan, S. Razavi, S. Seymour, P. Meraner, A. Gudlur, P.B. Stathopulos, M. Ikura, A. Rao, and P.G. Hogan. 2013. Initial activation of STIM1, the regulator of store-operated calcium entry. *Nat. Struct. Mol. Biol.* 20:973–981. http://dx.doi.org/10.1038/nsmb.2625